Research Square

Preprints are preliminary reports that have not undergone peer review.
They should not be considered conclusive, used to inform clinical practice,
or referenced by the media as validated information.

Bone marrow resident antigen presenting cells promote peripheral tolerance by inducing autoreactive regulatory T cells

Philipp Beckhove

philipp.beckhove@lit.eu

Leibniz Institute for Immunotherapy (LIT)

Chih-Yeh Chen

Leibniz Institute for Immunotherapy (LIT)

Felix Klug

German Cancer Research Center (DKFZ)

Siao-Han Wong

German Cancer Research Center (DKFZ)

Franziska Sanna

Leibniz Institute for Immunotherapy (LIT)

Sheena Pinto

German Cancer Research Center (DKFZ)

Alexander Wurzel

Leibniz Institute for Immunotherapy (LIT) https://orcid.org/0000-0003-3458-967X

Tomoyoshi Yamano

Kanazawa University https://orcid.org/0000-0001-8849-6239

Dania Riegel

Leibniz Institute for Immunotherapy (LIT)

Michael Delacher

University Medical Center Mainz https://orcid.org/0000-0002-6716-9156

Maria Dinkelacker

German Cancer Research Center (DKFZ)

Charles Imbusch

University Medical Center Mainz

Abdelrahman Mahmoud

German Cancer Research Center (DKFZ)

Roman Kurilov

German Cancer Research Center (DKFZ)

Miodrag Gužvić

University Hospital Regensburg https://orcid.org/0000-0001-8089-3969

Claudia Gebhard

Leibniz Institute for Immunotherapy (LIT)

Valentina Volpin

Leibniz Institute for Immunotherapy (LIT)

Ayse Nur Menevse

Leibniz Institute for Immunotherapy (LIT)

Yvonne Samstag

Institute of Immunology,Section Molecular Immunology, University of Heidelberg https://orcid.org/0000-0002-1536-2456

Pärt Peterson

Molecular Pathology Research Group, Institute of Biomedicine and Translational Medicine, University of Tartu https://orcid.org/0000-0001-6755-791X

Michael Rehli

University Hospital Regensburg https://orcid.org/0000-0003-3992-932X

Slava Stamova

University Hospital Regensburg

Maria Xydia

University Hospital Regensburg

Christoph Klein

University of Regensburg https://orcid.org/0000-0001-7128-1725

Mark Anderson

University of California San Francisco, San Francisco, CA, USA. https://orcid.org/0000-0002-3093-4758

Christian Schmidl

Leibniz Institute for Immunotherapy https://orcid.org/0000-0002-0522-202X

Markus Feuerer

Regensburg Center for Interventional Immunology

Benedikt Brors

German Cancer Research Center (DKFZ)

Article

Keywords: AIRE, Treg induction, tolerance, bone marrow

Posted Date: June 4th, 2026

DOI: https://doi.org/10.21203/rs.3.rs-9853026/v1

License: This work is licensed under a Creative Commons Attribution 4.0 International License.
Read Full License

Additional Declarations: (Not answered)

Abstract

Bone marrow (BM) harbors a large repertoire of regulatory T (Treg) cells, which are essential in hematopoiesis and peripheral tolerance. Treg cell accumulation in BM has been viewed as a consequence of preferential immigration of thymus-derived Treg cells. Here we report a subset of antigen presenting cells, which expresses the autoimmune regulator (Aire). These BM Aire-expressing cells resemble a subset of $CD138^{+}B220^{-}TACI^{+}Blimp\text{-}1^{+}MHC\text{-}II^{+}$ plasma cells (**p**lasma **c**ell-like **b**one **m**arrow **A**ire expressing **c**ells, *pc*-BMACs) and express tissue-restricted self-antigens. *pc*-BMACs present self-antigens to naïve $CD4^{+}$ T cells and can efficiently convert these into functionally competent $CD25^{+}Foxp3^{+}$ *bona fide* peripheral Treg cells (pTregs) capable of exerting immune suppression *in vitro* and *in vivo*. Aire expression may contribute to the tolerogenic function of *pc*-BMACs as it regulates the expression of genes involved in pTreg induction and function, including *Icosl* and retinoic acid synthesis-related genes. Our data demonstrate an Aire-expressing APC subset in the BM capable to promote peripheral tolerance by ectopically expressing tissue-restricted self-antigens and generating pTregs.

Introduction

As an indispensable primary and secondary lymphoid organ for hematopoietic homeostasis, the bone marrow (BM) harbors various types of cellular compartments for the development of hematopoietic stem and progenitor cells, as well as for the modulation of adaptive immune responses under physiological and inflammatory circumstances (1). For T cell homeostasis, BM niches provide survival signals including cytokines and cell adhesion molecules to antigen-specific memory T cells for their self-renewal and maintenance (2). Memory T cells specific to tumor-associated antigens are found in the BM of cancer patients (3, 4), and these tumor-specific memory T cells can be utilized for cancer immunotherapy such as adoptive T cell transfer therapy (5, 6). Apart from accommodating memory T cells, the BM also serves as a T-cell priming site, as BM-resident dendritic cells (DCs) can activate both $CD4^{+}$ and $CD8^{+}$ naïve T cells in the absence of other secondary lymphoid organs (7, 8). Moreover, regulatory T (Treg) cells are also enriched in the BM with a higher frequency than in spleen and lymph nodes (LNs) (9), and their immigration to BM depends on the balance of CXCL12 and G-CSF (10). As key regulators of both local and systemic immunity, Treg cells in BM play crucial roles in different types of diseases and manifest great value of clinical application. BM Treg cells are essential in immune hematopoiesis as they provide immune-privileged niches of hematopoietic stem cells (11), control IL-7 expression of BM stromal cells (12), regulate hematopoiesis (13), and are required for maintaining tolerance after stem cell transplantation (14). In addition to their local impact in BM, Treg cells migrate from BM to the periphery and regulate immune responses under inflammatory conditions. In cancer patients, tumor-specific Treg cells are detected in BM, and are selectively activated and upregulate the expression of the chemokine receptor S1P1, which leads to their emigration to peripheral tumor sites (15, 16). Thus, BM Treg cells comprise diverse functional clones covering a spectrum of self-antigens (10). However, it remains elusive how the diverse repertoire of Treg cells is generated in the BM. Hitherto, the BM has been largely viewed as a preferential site for the recirculation of Treg cells that are naturally

differentiated in the thymus (tTregs) (17). Here, we studied the possibility that the BM itself represents a site of peripheral Treg cell (pTreg) generation against self-antigens.

Promiscuous gene expression (pGE) is a hallmark of medullary thymic epithelial cells (mTECs) (18). These specialized cells are able to ectopically express tissue-restricted antigens (TRAs) and enable central tolerance for T cells by testing the specificities of thymocytes to prevent autoimmunity (19). The genetic regulation of pGE is predominantly controlled by the transcriptional regulator, autoimmune regulator (Aire) (20, 21). In addition to thymus, Aire expression has also been found in peripheral lymphoid organs like spleen and LNs, and these extrathymic Aire-expressing cells (eTACs) contribute to the maintenance of peripheral tolerance, mainly by depleting and anergizing autoreactive $CD8^+$ and $CD4^+$ T cells, respectively (22, 23). $Aire^+$ cells were found in LNs and referred to by various names including Janus cells (24), Thetis cells (25) and $Aire^+$ ILC3-like cells (26). Most recently, these three putatively distinct cell types have been summarized as RORγt-eTACs, referring to their RORγt-lineage (27). RORγt-eTACs demonstrate antigen-presenting cell (APC) features that likewise may regulate T cell responses through depletion of autoreactive T cells, or alternatively by inducing Tregs via TGFb activation. (26–28). Here we describe a novel cell subset, which expresses Aire in both murine and human BM. These Aire-expressing cells express a highly diverse repertoire of TRAs, and display a plasma cell-like surface phenotype ($CD19^{low}CD138^+B220^-Blimp\text{-}1^+IgM^+$) while maintaining a functional specialization in TRA expression.. They present TRAs via MHC-II to cognate $CD4^+$ T cells, and convert naïve $CD4^+$ T cells specific for Aire-regulated antigens to *bona fide* $CD25^+Foxp3^+$ Treg cells *in vitro* and *in vivo*. Treg cells induced in the BM express high levels of latency associated peptide (LAP) and show competent immune suppressive functions. Our data demonstrate for the first time that ectopic gene expression in BM Aire-expressing cells promotes peripheral tolerance by inducing Treg cell conversion.

Materials and Methods

Mice

Adig (22), Aire-HCO (29), 6.5 HA-TCR (30) and $Aire^{-/-}$ mice (31) have been described previously. Tyrp-1 TCR transgenic mice (32) [28] ($RAG1^{-/-}Tyrp1^{B-W}$ TRP-1 TCR) were purchased from The Jackson Laboratory. Both Adig and $Aire^{-/-}$ mice were backcrossed onto Balb/c background for more than 10 generations. Mice used in all experiments were maintained under specific pathogen-free condition. All mice were 6–12 weeks old and on Balb/c background, except mice used in experiments shown in Fig. 4D (C57BL/6 background, 6–12 weeks old) and in Fig. 2I (Balb/c background, 12–15 weeks old). Animal experiments were approved and regularly controlled by the authorities of local states (Regierungspräsidium Karlsruhe and Regierung von Unterfranken), in compliance with EU Directive 2010/63/EU.

Human samples

Collection of peripheral blood and BM samples from donors was performed in compliance with the ethics committee (approval reference number 70/99) of the University of Heidelberg upon signed consent. PBMCs and BM mononuclear cells were isolated from peripheral blood and bone marrow aspirate, respectively, using gradient centrifugation with Biocoll (Biochrom GmbH) according to manufacturer's protocol. Blood or bone marrow aspirate (40 to 45 ml) were gently placed on top of 15 ml of Biocoll solution, and then centrifuged for 20 min at 2,000 RPM at room temperature without forced deceleration. The interface containing mononuclear cells was carefully collected, washed with RPMI-1640 medium (Sigma-Aldrich) twice, and subjected to antibody staining for flow cytometric analysis.

Cell isolation from BM, spleen and thymus

Tibias, femurs and spleens were removed and ground, and cell suspension was passed through 100-μm cell strainer (Greiner), followed by lysis of erythrocytes. Thymic B cells and mTECs from WT, Adig or Aire-HCO mice were isolated as previously described (33). In brief, thymi of Aire-HCO mice were digested by Collagenase IV (Worthington), Dispase (Worthington) and DNaseI (Sigma-Aldrich), passed through 100-μm cell strainer (Greiner), and subjected to magnetic enrichment of $CD45^+$ cells using mouse CD45 microbeads (Miltenyi Biotec). $CD45^-MHC\text{-}II^+EpCAM^+Ly\text{-}51^-$ mTECs (from $CD45^-$ fraction) and $CD19^+MHC\text{-}II^+$ B cells (from $CD45^+$ fraction) were stained and sorted using FACSAria II (BD Biosciences).

Flow cytometric analysis and fluorescence-activated cell sorting

Antibodies against mouse antigens for flow cytometry and sorting are listed below: Aire (5H12, eBioscience), B220 (RA3-6B2, BioLegend), Blimp-1 (5E7, BioLegend), CD3 (17A2, BD Biosciences), CD4 (RM4-5, BD Biosciences), CD11b (M1/70, eBioscience), CD11c (N418, BioLegend), CD19 (1D3, BD Biosciences), CD25 (PC61, BioLegend), CD44 (IM7, BD Biosciences), CD45 (30-F11, eBioscience), CD45.1 (A20, BD Biosciences), CD45.2 (104, BD Biosciences), CD62L (MEL-14, BD Biosciences), CD80 (16-10A1, BioLegend), CD86 (GL1, BioLegend), CD138 (281-2, BioLegend), CTLA-4 (UC10-4B9, BioLegend), EpCAM (G8.8, BioLegend), F4/80 (BM8, BioLegend), Foxp3 (MF23, BD Biosciences), Helios (22F6, BioLegend), $H2\text{-}K^d$ (SF1-1.1, BioLegend), IgD (11-26c.2a, BioLegend), IgG1 (A85-1, BD Biosciences), IgG2a/b (R2-40, BD Biosciences), IgM (RMM-1, BioLegend), I-A/I-E (M5/114.15.2, eBioscience), LAG-3 (C9B7W, eBioscience), LAP (TW7-16B4, eBioscience), Ly-51 (BP-1, BD Biosciences), Nrp1 (3E12, BioLegend), PD-L1 (MIH5, eBioscience), PD-L2 (TY25, BD Biosciences), Sca-1 (D7, BD Biosciences), TACI (8F10, BioLegend). Anti-human AIRE antibody (clone 6.1) (34) was self-produced in lab. Antibodies against other human antigens are as follows: CD2 (RPA-2.10, BD Biosciences), EpCAM (9C4, BioLegend), HLA-DR (L243, eBioscience). Viability dyes used for excluding dead cells were 7-AAD (BioLegend), Yellow LIVE/DEAD Fixable Dead Cell Stain Kits (Molecular Probes), Zombie Aqua Fixable Viability Kit (BioLegend), and Zombie NIR Fixable Viability Kit (BioLegend). Single cell suspension (1–2×10^6 cells/100 μl) was incubated with anti-mouse CD16/32 antibody (93, BioLegend) for 15 min on ice, followed by incubation with antibodies against surface markers for 30 min on ice. After subsequent

wash, cells were stained with viability dye, and all cells analyzed were gated on viable cells (viability dye-negative). For intracellular staining, after viability staining, cells were fixed and permeabilized using Foxp3/Transcription Factor Fixation/Permeabilization Concentrate and Diluent (eBioscience) according to manufacturer's protocol, and then incubated with antibodies against intracellular antigens for 30 min on ice. FACSCanto II, LSR II or FACSLyric (BD Biosciences) flow cytometers were used for fluorescence measurement, and FACSAria II (BD Biosciences) was used for cell sorting. The analysis was performed using FlowJo (Tree Star) software.

Immunofluorescence

After Adig or WT Balb/c mice were euthanized, thymi were dissected and embedded in Tissue-Tek (Sakura) and frozen at -20°C. Femurs and tibias were dislocated and the attached muscle was removed. Epiphyses of the bones were gently removed, and marrow tissue was carefully pushed out from the bones with PBS by 27-gauge needle, without disrupting the marrow tissue. The intact marrow tissue was then embedded and frozen as the thymi tissue. Cryo-sections (5 μm) of thymus and BM tissue were fixed with cold acetone for 10 min, and then blocked with 10% goat serum for 30 min at room temperature. Tissue was incubated with anti-Aire (5H12, eBioscience), anti-CD4 (H129.19, BD Biosciences), anti-CD8 (53 – 6.7, BD Biosciences), anti-CD19 (1D3, BD Biosciences), anti-GFP (polyclonal ab290, abcam) or anti-MHC-II (ER-TR3, abcam) primary antibodies for 1 hour at room temperature. After washing with Tween-20/PBS and PBS, tissue was incubated with goat anti-rat or goat anti-rabbit secondary antibodies (Molecular Probes). Stained slides were mounted in DAPI-containing Fluoromount-G mounting medium (eBioscience), and visualized by Axio Imager Z1 (Carl Zeiss). Merging and contrast-adjustment were applied equivalently to experimental and control groups using ImageJ software.

Real-Time PCR

Aire-GFP^{+} BM cells were isolated and sorted from Adig mice by FACS according to GFP expression, and Adig mTECs were isolated and sorted as described above. RNA from the sorted cells was extracted using RNeasy Mini Kit (Qiagen). After quantification, RNA was reverse transcribed using QuantiTect Reverse Transcription Kit (Qiagen) according to manufacturer's protocol. *Aire* and *Actb* gene expression was detected by 7300 Real-Time PCR System (Applied Biosystems) using QuantiFast SYBR Green PCR Kit (Qiagen) according to manufacturer's protocol with the following primer sets: *Aire* forward (5'-TGCAGGAGATCCCCAGTG-3'), *Aire* reverse (5'-TGGGACAGGTTCTGTTGGAC-3'), *Actb* forward (5'-ACGGCCAGGTCATCACTATTG-3'), and *Actb* reverse (5'-AGGATTCCATACCCAAGAAGGAA-3'). ΔΔCt values was calculated for relative expression.

Multispectral imaging flow cytometry

BM cells were isolated from Adig mice, and stained with antibodies as described above. Single cell suspension (1–2×10^{6} cells/60 μl PBS) was subjected to ImageStream IS100 (Amnis) and analyzed by

INSPIRE software (Amnis).

Assay for transposable-accessible chromatin with sequencing (ATAC-seq)

BM cells from Adig mice (shown in Fig. 2E-G and S2A), and T cell subsets (shown in Fig. 6G and 6H) were sorted and chromatin accessibility mapping was performed using the ATAC-seq method as previously described (35), with minor adaptations. Briefly, in each experiment 1,500 – 50,000 sorted cells were pelleted by centrifuging for 10 min at 4°C at 500 x g. After centrifugation, the pellet was carefully lysed in 50 µl resuspension buffer supplemented with NP-40 (Sigma), Tween-20 and Digitonin (10 mM Tris-HCl pH 7.4, 10 mM NaCl, 3 mM $MgCl_2$, 0.1 % N-40, 0.1 % Teen-20, 0.01 % Dgitonin), and incubated for 3 minutes on ice. Then, 1 ml of ice-cold resuspension buffer supplemented with 0.1 % Teen-20 was added, and the sample was centrifuged at 4°C at 500 x g for 10 minutes. The supernatant was discarded, and the cell pellet was carefully resuspended in the transposition reaction (25 µl 2 x TD buffer (Illumina), 2.5 µl TDE1 (Illumina), 16.5 µl PBS, 5 µl nuclease-free water, 0.5 µl 1% Digitonin (Promega), 0.5 µl 10% Tween-20 (Sigma)) for 30 min at 37°C on a shaker at 1000 rpm. Following DNA purification with the Clean and Concentrator-5 kit (Zymo) eluting in 23 µl, 2 µl of the eluted DNA was used in a quantitative 10 µL PCR reaction (1.25 µM forward and reverse custom Nextera primers (35), 1x SYBR green final concentration) to estimate the optimum number of amplification cycles with the following program 72°C 5 min; 98°C 30 s; 25 cycles: 98°C 10 s, 63°C 30 s, 72°C 1 min; the final amplification of the library was carried out using the same PCR program and the number of cycles according to the Cq value of the qPCR. Library amplification using custom Nextera primers was followed by SPRI size selection with AmpureXP beads to exclude fragments larger than 1,200 bp. DNA concentration was measured with a Qubit fluorometer (Life Technologies). The libraries were sequenced using the Illumina NextSeq550 platform using a High Output Kit (75 cycles) in paired-end mode.

For Preprocessing and analysis of ATAC-seq data, ATAC-seq reads were trimmed using Skewer (36) and aligned to the mm10 assembly of the murine genome using Bowtie2 (37) with the "-very-sensitive" parameter and a maximum fragment length of 2,000. Duplicate and unpaired reads were removed using the sambamba (38) "markdup" command, and reads with mapping quality > 30 and alignment to the nuclear genome were kept. All downstream analyses were performed on these filtered reads. For visualization purposes only, coverage files from filtered bam files were produced using bedtools genomeCoverageBed command (39). Each position was normalized by dividing to the total library size and multiplying by 10^6, followed by conversion to a bigwig using the bedGraphToBigWig command from the UCSC genome browser tools.

For Bioinformatic analysis of chromatin accessibility data, peak calling was performed using HOMER (40) with the following approach: Two different peak sets were called, once we used the options "-style factor -fragmentLength 150 -size 250 -minDist 250 –L 4 –fdr 0.0001 -tbp 1" parameters, to identify highly robust small regions of open chromatin, and in a second approach we used the parameters "-region -

fragmentLength 150 -size 150 -minDist 250 -L 4 -fdr 0.0001 -tbp 1" to identify larger regions of open chromatin. The two peak sets were then merged using the bedtools intersect function with the "-u" option to create the peak set that was used for downstream analysis. For the analysis of sample sets we always created a consensus region set by merging the called peaks from all involved samples using bedtools, and we quantified the accessibility of each region in each sample by counting the number of reads from the filtered BAM file that overlapped each region. Peaks overlapping blacklisted features as defined by the ENCODE project (41) were discarded. To normalize the chromatin accessibility signal across samples, we performed quantile normalization followed by GC content normalization by regression using the cqn R package (42). Principal component analysis (PCA) was performed using the R package *prcomp* on the normalized chromatin accessibility values of all significant chromatin-accessible regions across all samples in the respective sample sets. DESeq2 (43) was used on the raw count values for each sample and regulatory element to identify differential chromatin accessibility between samples. Significant regions were defined as having an FDR-corrected *p*-value (Benjamini-Hochberg) below 0.05, an absolute $\log_2$ fold change above 1, and a mean accessibility equal or greater than 10.

BM chimera

For the generation of reciprocal BM chimeras, CD45.1$^+$ WT congenic Balb/c or CD45.2$^+$ Adig recipient mice were irradiated twice at 450 rad with an interval of 3 hours, and i.v. injected with 1×10^7 BM mononuclear cells from CD45.2$^+$ Adig or CD45.1$^+$ WT congenic Balb/c mice, respectively. After at least 8 weeks of reconstitution of hematopoietic system, recipient mice were euthanized, and BM mononuclear cells were isolated. The chimerism was confirmed using CD45 congenic marker expression by flow cytometric analysis, and more than 98.9% of CD45$^+$ cells had the congenic CD45 phenotype of the donor mice. For the preparation of recipient mice with HA-expressing hematopoietic cells, CD45.1$^+$CD45.2$^+$ WT Balb/c mice were irradiated twice at 450 rad with an interval of 3 hours, and intravenously injected with 1×10^7 BM mononuclear cells from CD45.1$^+$CD45.2$^+$ Aire-HCO or CD45.1$^+$CD45.2$^+$ WT Balb/c mice. Further manipulations were performed at least 8 weeks after the BM transplantation.

Gene expression microarray

For TRA expression profile (**Figure S3B** and **S3C**), BM Aire-GFP$^+$ cells were isolated and sorted from Adig mice, and mTECs from Adig mice were isolated and sorted according to the method described above. RNA from the sorted cells was extracted using RNeasy Mini Kit (Qiagen). Quantified RNA was tested for quality using Agilent 2100 Bioanalyzer (Agilent Technologies). RNA was amplified using Ovation RNA Amplification System (44) (NuGEN) and subjected to MouseRef-8 v2.0 Expression BeadChip (Illumina). Expression signals were normalized by quantile normalization.

For comparing BMACs and plasma cells (Fig. 5A, 5B, S5B and S5C), Aire-GFP$^+$ cells and plasma cells were isolated and sorted from BM of Adig mice by FACS. RNA of sorted cells was isolated and amplified using μMACS SuperAmp Kit (Miltenyi Biotec) followed by Klenow labeling (Fermentas) with random

octamer (Enzo Life Sciences GmbH) according to manufacturer's protocol, and subjected to MouseRef-8 v2.0 Expression BeadChip (Illumina). The corresponding chip annotation file is obtained from Illumina website. Raw data are processed with R using limma package. First, normalization was performed locally and globally. With normexp background correction method, spots within each sample were corrected by local background. A subsequent quantile normalization was performed for global normalization across all samples. Second, preprocessing was applied based on whether a gene is expressed in the cohort. Based on the spot detection *p*-value returned from detectionPValues function, genes not expressed in any sample ($P < 0.05$) were excluded from further analysis. Lastly, differential expression analysis was performed. Expression of each gene was fitted with a linear model using lmFit function, then eBayes function applies empirical Bayes method to stabilize standard deviations between genes. Benjamini, Hochberg multiple correction method is used to correct differential expression *p*-values. The significantly differentially expressed genes were then subject to functional enrichment analysis with R package EGSEA.

RNA-seq for transcriptome analyses

For bulk RNA-seq, *Aire*$^{+/+}$ and *Aire*$^{-/-}$ *pc*-BMACs were sorted into RLT buffer of RNeasy Micro Kit (Qiagen) and RNA was isolated according to the manufacturer's protocol. Libraries were generated using Smart Seq v4 Ultra Low Input RNA Kit (Clontech), and sequenced (single-ended 85 bp) on a NextSeq 500/550 (Illumina). Single-end reads were processed by OTP pipeline (45) [41] to obtain gene counts. The pipeline aligned reads to reference genome GRCm38 (mm10) using STAR (v2.5.3a), and the resulting mapped reads number ranged from 64M to 75M. The alignment is summarized into gene counts using featureCounts (v1.5.1) and gene model (GENCODE v12). Differential gene expression was performed with DESeq2 (v1.22.2). We start with protein-coding genes having count greater than 10 when combining all four samples, and perform DESeq2 with default settings. Hypergeometric tests were used to test the significant enrichment of TRA in the differentially expressed genes.

For single cell RNA-seq, single *Aire*$^{+/+}$ and *Aire*$^{-/-}$ *pc*-BMACs were sorted into lysis buffer containing 0.2% (V/V) Triton X-100 (Sigma) and 2 U/µl of RNase inhibitor (Clonetech). cDNA libraries were prepared using SMART-seq2 as previously described (46) [42], and sequenced (single-ended 50 bp) on a HiSeq 3000/4000 (Illumina). Alignment of single-end reads to the reference genome GRCm38 (mm10) was performed using STAR (v2.5.2b). Around 1M to 20M (median 4.7M) uniquely mapped reads were yield from the 186 cells sequenced. Gene expression was summarized using featureCounts (v1.5.1) and gene model (GENCODE v15). To allow for comparison across cells, total counts at the cell-level were normalized to a fixed scale factor of 250K. In the subsequent analysis, genes having non-zero counts were considered expressed in a cell.

Antigen presentation assay

Aire-expressing cells from BM and spleens were sorted from Aire-HCO or Adig mice by FACS according to human CD2 (hCD2) or GFP expression, respectively, and mTECs from Aire-HCO mice were isolated

and sorted according to the method described above. The sorted APC subsets were co-cultured with 2×10^4 A5 T-hybridoma cells (47) at designated APC:TC ratio for 17 h, and $CD4^+$ A5 cells were analyzed for GFP expression as previously described (30).

BrdU incorporation assay

CD25-depleted naïve $CD4^+$ T cells were isolated by negative selection using MojoSort Mouse CD4 Naïve T Cell Isolation Kit (BioLegend) from the spleens of Tyrp1 TCR transgenic mice. Naïve Tyrp1-specific $CD4^+$ T cells were co-cultured with $CD11c^+$ dendritic cells from *Tyrp1*$^{B-W}$ mice, or *pc*-BMACs from WT B6 mice sorted according to **Figure S1E** at 20:1 APC:TC ratio with recombinant murine IL-2 (20 ng/ml, Peprotech) and BrdU (1 mM, BD Biosciences). For blocking MHC-II, 10 μg/ml of anti-MHC-II antibody (clone Y-3P, BioXCell) or mouse IgG2a isotype control antibody (clone MOPC-173, BioLegend) was used. Four days after culture, cells were collected and subjected to surface marker and BrdU staining according to the manufacturer's protocol.

In vitro Treg induction

CD25-depleted naïve $CD4^+$ T cells were isolated by negative selection using MojoSort Mouse CD4 Naïve T Cell Isolation Kit (BioLegend) from the spleens of $CD45.2^+$ 6.5 HA-TCR mice or $CD45.1^+$ WT Balb/c mice. For *in vitro* Treg induction by TGFβ1, isolated naïve $CD4^+$ T cells were stimulated using Mouse T-Activator CD3/CD28 beads (Gibco) at 1:1 cell:bead ratio, with recombinant murine recombinant mouse TGFβ1 (5 ng/ml, R&D Systems) for 4 days.

For *in vitro* Treg induction by Aire-expressing cells, Aire-GFP^+ cells or Aire-$hCD2^+$ cells (total cells, *pc*-BMACs, or non-*pc*BMACs) from BM were sorted from Adig or Aire-HCO mice, respectively. Sorted APCs (2×10^4) were co-cultured with 2×10^4 pooled naïve $CD4^+$ T cells with recombinant murine IL-2 (20 ng/ml, Peprotech) for 4 days, and $CD45.2^+$ HA-specific $CD4^+$ T cells and $CD45.1^+$ polyclonal $CD4^+$ T cells were analyzed by flow cytometry. For blocking TGFβ1, 20 μg/ml of anti-human/mouse TGFβ1 antibody (clone 19D8, BioLegend) or mouse IgG1 isotype control antibody (clone MOPC-21, BioLegend) was used.

Adoptive T cell transfer

CD25-depleted $CD4^+$ T cells were isolated by negative selection using MojoSort Mouse CD4 Naïve T Cell Isolation Kit (BioLegend) from the spleens of $CD45.2^+$ 6.5 HA-TCR or $CD45.1^+$ WT Balb/c mice, pooled together at 1:1 ratio, and labeled with 5 μM carboxyfluorescein succinimidyl ester (CFSE) for 5 min at room temperature (48). The labeled cells (1×10^7 per recipient mouse) were i.v. injected into $CD45.1^+CD45.2^+$ host mice, which were reconstituted with Aire-HCO or WT BM cells at least 8 weeks before the transfer of naïve $CD4^+$ T cells. On day 3 and day 14 post transfer, BM cells and splenocytes were isolated and analyzed by flow cytometry.

Sequencing of bisulfite-DNA amplicons

T cell subsets (shown in Fig. 6E and 6F) were sorted directly into FACS buffer and then lysed with buffer ATL and proteinase K (Qiagen QIAamp DNA Micro Kit) for one hour at 56°C. Buffer ATL and AL with carrier RNA were added and sample stored at -80°C until further processing. To isolate genomic DNA, samples were heated to 90°C for 30 minutes followed by column-based DNA isolation according to manufacturer's protocol (Qiagen QIAamp DNA Micro Kit). DNA was eluted in 40 µl buffer AE and sodium bisulfite conversion was performed (Qiagen EpiTect Plus DNA Bisulfite Kit). Bisulfite-converted DNA was used to amplify regions of interest (49) with the following PCR conditions: 4 µl bisulfite-converted DNA, 0.5 µl forward primer (10 µM), 0.5 µl reverse primer (10 µM), 5 µl 2X PCR buffer, 0.1 µl dNTPs and 0.1 µl hot-start Taq polymerase (PCR buffer, dNTPs and Taq from: ZymoTaq DNA Polymerase Kit #E2002). To detect *Foxp3* methylation at the Treg-specific demethylated region, we used a forward primer TGGGTTTTTTTGGTATTTAAGAAAG and a reverse primer AAAAAACAAATAATCTACCCCACAA. To detect *Il2ra* gene methylation, we used a forward primer TTTTAGAGTTAGAAGATAGAAGGTATGGAA and a reverse primer TCCCAATACTTAACAAAACCACATAT. For *Ikzf2* gene methylation, we used a forward primer AGGATGGTTTTTATTGAAGGTGAT and a reverse primer ATACACACCAAACAAACACTACACC. For *Ctla4* gene methylation, we used a forward primer TGGTGTTGGTTAGTAGTTATGGTGT and a reverse primer AAATTCCACCTTACAAAAATACAATC. For *Tnfrsf18* gene methylation, we used a forward primer GAGGTGTAGTTGTTAGTTGAGGATGT and a reverse primer AACCCCTACTCTCACCAAAAATATAA. PCR was initiated with 95°C for 10 minutes, followed by 40 cycles with denaturation (95°C-30sec), annealing (56°C-30sec) and elongation (72°C-30sec) completed with a final elongation step (72°C for 7 minutes). PCR products were combined, pre-purified with AMPure XP beads (Beckman Coulter) and indexed for Illumina-based sequencing (NEBNext Ultra II DNA Library Prep Kit for Illumina with NEBNext Multiplex Oligos for Illumina). Samples were pooled in an equimolar ratio and supplemented with an unindexed PhiX spike-in (50% spike-in, Illumina). Sequencing was performed on an Illumina MiSeq with a Reagent Nano kit v2 and 500 cycles of PCR (Illumina). Indexed reads were aligned to the respective gene region and the mouse mm10 genome, followed by CG methylation calling and raw data table exporting using a customized code. For *Foxp3*, following CG dinucleotides were analyzed and plotted CG1 X:7,583,950; CG2 X:7,583,986; CG3 X:7,584,002; CG4 X:7,584,036; CG5 X:7,584,063; CG6 X:7,584,068. For *Il2ra*, following CG dinucleotides were analyzed and plotted CG1 2:11,645,653; CG2 2:11,645,705; CG3 2:11,645,718; CG4 2:11,645,738. For *Ikzf2*, following CG dinucleotides were analyzed and plotted CG1 1:69,670,284; CG2 1:69,670,291; CG3 1:69,670,370; CG4 1:69,670,377; CG5 1:69,670,385.

Ex vivo Treg suppression assay

$CD45.1^{-}CD45.2^{+}CD4^{+}CD25^{+}LAP^{+}$ HA-specific donor Treg cells, $CD45.1^{+}CD45.2^{+}CD4^{+}CD25^{+}Nrp1^{+}$ host Treg cells, and $CD45.1^{+}CD45.2^{+}CD4^{+}CD25^{+}Nrp1^{+}$ host Tconv cells were sorted from the BM of $CD45.1^{+}$ $CD45.2^{+}$ host mice 14 days post naïve T cell transfer. These suppressor cells were co-cultured at different ratio with CFSE-labeled naïve $CD4^{+}$ T cells (1×10^{4}) isolated from $CD45.1^{+}CD45.2^{-}$ WT Balb/c mice. T cells were stimulated using Mouse T-Activator CD3/CD28 beads (Gibco) at 1:1 cell:bead ratio for 4 days and the reduction of CFSE intensity of $CD4^{+}CD45.1^{+}CD45.2^{-}$ T cells was analyzed by flow cytometry.

In vivo cytotoxicity

$CD45.1^+CD45.2^+$ 6.5 HA-TCR mice were immunized twice (2-week interval) with 100 μg HA-peptide (SVSSFERFEIFPK, synthesized by thinkpeptides) with 10 μg lipopolysaccharide (Sigma-Aldrich) and 10 μg polyinosinic-polycytidylic acid (Sigma-Aldrich) via intraperitoneal (i.p.) injection. One week after the second immunization, effector T cells were isolated from the spleens and BM of the immunized mice using EasySep Mouse Memory $CD4^+$ T Cell Isolation Kit (STEMCELL Technologies). Recipient mice (previously reconstituted with WT or Aire-HCO BM, and transferred with naïve HA-specific $CD4^+$ T cells, as described above) received 3×10^6 effector T cells via i.v. injection at 14 days post naïve T cell transfer. One day later, BM cells and splenocytes isolated from $CD45.1^+$ WT Balb/c mice were pooled together at 1:1 ratio and labeled with 5 or 0.5 μM of CFSE for 5 min at room temperature. The $CFSE^{high}$ cells were pulsed with 20 μM (31.5 μg) HA-peptide for 2 hours at 37°C, and the $CFSE^{low}$ cells were incubated without peptide. After 2 washes with PBS, the peptide-loaded $CFSE^{high}$ and unloaded $CFSE^{low}$ target cells were mixed at 1:1 ratio and transferred into the recipient mice (5×10^5 cells/mouse). Eighteen hours later, recipient mice were sacrificed, and BM cells and splenocytes were isolated for flow cytometric analysis. $CD45.1^+CD45.2^-B220^+$ cells were gated for analyzing the proportions of $CFSE^{high}$ and $CFSE^{low}$ target cells. Cytotoxicity was calculated as follows:

$$\% \text{ specific cytotoxicity} = 100\% \times (1-(CFSE^{low} / CFSE^{high})_{control} / (CFSE^{low} / CFSE^{high})_{experimental}).$$

Statistics

Unless stated otherwise, statistical significance was assessed using two-tailed Student's *t* test with unequal variance. Data are shown in mean ± SEM.

Data availability

The data, code and associated protocols that support the findings of this study are available from the corresponding authors upon request. The data reported in this paper have been deposited in the Gene Expression Omnibus (GEO) database under accession number GSE136650.

Results

Aire is expressed in both murine and human BM

BM is a central reservoir of Treg cells. We hypothesized that a local source of self-antigens serves to generate or maintain peripherally-induced Treg cells. To address this question, we harnessed Adig transgenic mice in which the GFP reporter protein is driven by a murine *Aire* locus (22). Immunofluorescence demonstrated that Aire-GFP reporter protein was expressed in both the thymus and BM (Fig. 1A). In order to further confirm the expression of Aire in the BM-resident Aire-expressing cells (termed BMACs henceforth), we sorted Aire-GFP^+ cells from the thymus and BM of Adig mice and performed Real-Time quantitative PCR to determine the expression level of *Aire* transcript. As shown in

Fig. 1B, BMACs expressed *Aire* mRNA, which was not detected in Aire-GFP$^-$ BM cells, albeit the expression level in BMACs was approximately 8-fold lower than in mTECs. Immunocytochemistry was performed on sorted Aire-GFP$^+$ cells to assess Aire protein expression. The pattern of Aire expression exhibited puncta-like structure in the nuclei (Fig. 1C), which was also observed in the BM tissue of WT Balb/c mice (Fig. 1D), resembling the Aire expression pattern in mTECs (50). BMACs and mTECs also shared other common features, such as the expression of MHC-II and EpCAM (Fig. 1D and 1E). Moreover, to assess the presence of BMACs in human BM we further isolated mononuclear cells from human blood and BM donors and conducted flow cytometric analysis after intracellular staining for AIRE protein. As depicted in Fig. 1F, we detected AIRE expression in human BM, and in keeping with our findings in murine models, human BM AIRE-expressing cells expressed EpCAM and low levels of MHC-II. In blood derived mononuclear cells, however, AIRE was undetectable, demonstrating that human AIRE-expressing cells are significantly enriched in BM compared to the blood (Fig. 1G). Thus, AIRE expression is present in MHC-II$^+$EpCAM$^+$ cells in the BM in both murine and human.

The majority of Aire-expressing cells in the BM has a plasma cell-like phenotype

To further confirm the cell identity of BMACs, we performed surface marker screening by flow cytometric analysis. BMACs expressed the hematopoietic marker CD45 (Fig. 2A), suggesting their identity as hematopoietic cells. While no expression of CD11b and CD11c was detected on BMACs (**Figure S1A**), they manifested characteristics of plasma cells (CD19^{low}B220$^-$CD138$^+$TACI$^+$Blimp-1$^+$, Fig. 2A and 2B). Interestingly, the vast majority of BMACs expressed surface IgM (sIgM), but not sIgD, sIgG1, sIgG2a and sIgG2b (Fig. 2A and S1B), reminiscent of a fraction of cytokine-secreting plasma cells that express membrane-bound IgM and MHC-II (51). Of note, Aire protein was detected in 22.1 ± 3.5% of MHC-II$^+$TACI$^+$ BM cells of *Aire*$^{+/+}$ mice, but not in the counterpart BM cells of *Aire*$^{-/-}$ mice (Fig. 2C and S1C). Furthermore, BMACs also expressed Sca-1, which was recently described as a plasma cell marker (52) (**Figure S1D**). In the BM, B220$^-$CD138$^+$TACI$^+$IgM$^+$ cells (henceforth called *plasma cell-like* BMACs, *pc*-BMACs) made up more than 60% of total Aire-GFP$^+$ cells (Fig. 2D), and more than 90% of B220$^-$CD138$^+$TACI$^+$IgM$^+$ cells showed Aire-GFP expression (**Figure S1E**), indicating *pc*-BMACs are the major population of Aire-expressing cells in the BM. Of note, around 20% of Aire$^+$B220$^-$CD138$^+$TACI$^+$ BM cells did not express IgM, and a fraction of BM Aire-GFP$^+$ cells is B220$^+$ (around 20%), indicating that *pc*-BMACs, albeit being the major Aire$^+$ population, are not the sole population expressing Aire.

To systemically examine their molecular cell identity, we sorted *pc*-BMACs from Adig mice for open chromatin profiling using ATAC-seq. Differential peak calling of the sequences obtained from ATAC-seq showed that *pc*-BMACs have significantly higher accessibility of the *Aire* promoter (Chromosome 10: 78,043,200 – 78,044,001) than BM plasma cells and B cells (Fig. 2E). In line with the results of flow cytometric protein detection, there was no significant difference of *Prdm1* (*Blimp-1*), *Xbp1*, and *Sdc1* (*Cd138*) loci between *pc*-BMACs and BM plasma cells (Fig. 2E and S2A), suggesting a plasma cell

signature (53, 54). In contrast, BM B cells showed significantly lower accessibility of these loci than *pc*-BMACs, while the *Pax5* locus, indicative for early B cells, was significantly more accessible in BM B cells than in *pc*-BMACs (Fig. 2E and S2A). Principal component analysis (PCA) and unsupervised clustering of the overall open chromatin profile of *pc*-BMACs indicated a closer lineage relationship of *pc*-BMACs to plasma cells than to the B cell lineage (Fig. 2F and 2G). It is noteworthy that open chromatin profiling also showed distinct features of *pc*-BMACs compared to classical plasma cells, suggesting their functional difference. Moreover, in BM chimeras where lethally irradiated WT mice received Adig BM cells (Adig → WT) and Adig mice received WT BM cells (WT → Adig), BMACs were observed in both reciprocal BM chimeras, indicating and irradiation resistance (55), respectively (Fig. 2H and S2B). In accordance, BMACs were observed after transfer of Adig BM into WT recipients, indicating hematopoietic origin. The Aire-GFP$^+$ cells observed in WT recipient mice which received Adig BM cells could derive from *de novo* generation, as well as from the remaining Aire-GFP$^+$ cells in donor cells. Of note, we still observed some BMACs in lethally irradiated Adig BM, even after reconstituted by WT BM, which is in line with the well-described irradiation resistance of plasma cells. These attributes of plasma cell phenotype fall in line with the fact that the frequencies of BMACs were significantly reduced in *Rag2*$^{-/-}$ mice (Fig. 2I and S2C). Residual Aire-GFP$^+$ cells were still detectable in the BM of *Rag2*$^{-/-}$ mice, suggesting that a minor fraction of BMACs is *Rag2*-independent. The *Rag2*-dependent Aire$^+$ cells showed low to intermediate levels of MHC-II expression (**Figure S2D**), consistent to the human BM AIRE$^+$ cells (Fig. 1F), and they expressed CD138 and IgM. On the contrary, the *Rag2*-independent counterpart showed high expression levels of MHC-II, which was not detected in human BM, and they did not show features of plasma cells. Taken together, these results demonstrated that Aire is expressed by a hitherto undescribed MHC-II$^+$EpCAM$^+$IgM$^+$ subset of cells in the BM, that share similiarities with certain plasma cells.

BMACs ectopically express tissue-restricted antigens

Aire plays a central role in controlling pGE in mTECs and eTACs (21, 56). We therefore examined the function of Aire as a transcription factor to promote ectopic TRAs expression in BM. BMACs and mTECs of Adig mice were sorted according to Aire-GFP expression (**Figure S3A**) and subjected to bulk gene expression array analysis. This revealed that BMACs expressed 721 genes which are classified as TRAs according to previously described criteria (57, 58), and 634 genes of these TRAs were commonly expressed by both mTECs and BMACs, whereas 87 of them were exclusively expressed in BMACs (**Figure S3B** and **Table S1**). Of note, among the TRAs expressed by BMACs, we found numerous self-antigens associated to various autoimmune diseases, such as *CNP* for multiple sclerosis(59) and *Col5a1* for rheumatoid arthritis (60), as well as tumor-associated testis antigens such as *Mage-d1* and *Mage-e1*, and the melanoma-associated antigen *Tyrp1*. The TRA genes expressed by BMACs represented highly diverse tissue types (**Figure S3C**). To further delineate the repertoire of TRA genes expressed in *pc*-BMACs on single cell level, we sorted single *pc*-BMACs and generated cDNA libraries using Smart-seq2 (46). In transcriptome analysis of 186 single *pc*-BMACs derived from two individual mice, 1883 and 1847 TRA genes were detected in *pc*-BMACs from each individual mouse, respectively, revealing a large

overlap of TRAs expressed in *pc*-BMACs of different mice, adding up to a total of 2045 different TRA genes (51% of all TRA genes described (57, 58), Fig. 3A). Most of these TRA genes (more than 99%) were detected previously in single mature mTECs (61), and when we compared the TRAs expressed by *pc*-BMACs to the Aire-dependent genes found in mTECs according to a previous study (61), we found only 210 TRA genes in *pc*-BMACs were Aire-dependent in mTECs, suggesting most of the TRAs expressed by *pc*-BMACs are Aire-independent. Similar to the mosaic pattern of TRA expression in mTECs (62, 33), most of TRA genes were expressed in small fractions of *pc*-BMACs (Fig. 3B). Consistent with our previous data, *pc*-BMACs expressed *Aire* and *MHC-II* (*H2-Ab1*) transcript, as well as genes characteristic for plasma cells such as *Xbp1* and *Irf4*, with low level of *Cd19* (Fig. 3C). In order to determine the scope of Aire-regulated genes, we compared deep sequencing data of bulk-sorted $Aire^{+/+}$ and $Aire^{-/-}$*pc*-BMACs. As shown in **Table S2** and Fig. 3D, 135 genes were differentially regulated by Aire in *pc*-BMACs. These genes were significantly enriched for genes encoding TRAs ($P = 0.0092$). The Aire-induced genes were enriched for TRAs ($P = 0.00064$), whereas the Aire-repressed genes showed no significant enrichment for TRAs, indicating a positive impact of Aire on TRA expression in *pc*-BMACs. Of note, only a few Aire-induced TRA genes overlapped with the ones expressed by other Aire-expressing hematopoietic cell subsets (1 TRA gene shared with thymic B cells, 2 with eTACs, 1 with ILC3-like $Aire^{+}$ cells, **Table S2**) (22, 26, 29). While all together only a minor fraction of TRA genes were regulated by Aire in *pc*-BMACs, in addition to TRA upregulation, Aire also induced genes related to Treg induction such as *Icosl* (63, 64)and retinoic acid (RA) synthesis-related genes, *Aldh1b1* and *Aldh1a2* (65, 66)(Fig. 3D and **Table S2**), suggesting an immune regulatory role of Aire on top of induction of TRA expression in *pc*-BMACs. These data indicate that *pc*-BMACs express TRA genes which are largely Aire-independent, and Aire regulates a minor fraction of TRAs but also immune regulatory genes in *pc*-BMACs.

BMACs present transgenic Aire-driven antigen and endogenous TRA to $CD4^{+}$ T cells

Based on the findings that BMACs express MHC-II and TRAs, we hypothesized BMACs are able to present TRAs to $CD4^{+}$ T cells. Multispectral imaging flow cytometric analysis revealed that MHC-II, but not MHC-I, was expressed in clusters on BMACs, which suggests the competence of BMACs to present antigens via MHC-II (67) (Fig. 4A). In addition, in the BM parenchyma BMACs resided in the vicinity of $CD4^{+}$ T cell clusters (Fig. 4B), indicating an *in situ* interaction between BMACs and $CD4^{+}$ T cells. Close contact of BMACs with $CD8^{+}$ T cells or with $CD19^{+}$ B cells was not observed. In order to validate the function of BMACs to present endogenous antigens, we next employed the Aire-HCO transgenic mouse system, in which a model antigen (hemagglutinin, HA) and a reporter protein surface marker (human CD2, hCD2) are expressed under the control of the Aire promoter (29, 30). We sorted BMACs, mTECs, thymic B cells (29) and peripheral Aire-expressing cells (26, 22, 23) according to hCD2 expression (**Figure S4A**), and co-cultured them with A5 T-hybridoma cells, which express a TCR specific for HA peptide:I-E^{d} complex, and carry a GFP expression cassette driven by the IL-2 promoter and NFAT binding sites reporting stimulation of the TCR (30). As shown in Fig. 4C, BMACs were able to present Aire-

regulated antigen and induced NFAT-GFP expression via TCR signaling in A5 hybridoma cells. BMACs induced NFAT-GFP expression to a higher extent than Aire-hCD2$^+$ cells in the spleen, albeit less efficient than mTECs and thymic B cells. In order to confirm the capability of *pc*-BMACs to present not only model antigens but also endogenous TRAs to cognate CD4 T cells, we exploited TCR transgenic mice which recognize MHC-II-restricted epitope of Tyrp1 (32) whose expression was detected in BMACs. We sorted *pc*-BMACs from WT C57BL/6 mice (sorting strategy as in **Figure S1E)**, and co-cultured them with purified naïve Tyrp1-TCR transgenic CD4$^+$ T cells (**Figure S4B**). Upon co-culture with WT *pc*-BMACs, Tyrp1-specific CD4$^+$ T cells showed marked incorporation of 5-bromo-2′-deoxyuridine (BrdU), indicating the induction of proliferation (68) (Fig. 4D). This was not the case when either TCR:MHC-II interaction was blocked by anti-MHC-II antibody, or when dendritic cells from Tyrp1-deficient (*Tyrp1*$^{B-w}$) mice (32) were used as APCs. These data indicate a MHC-II-dependent activation of Tyrp1-specific T cells by *pc*-BMACs. Taken together, these results demonstrate that BMACs are competent APCs and can induce the activation of CD4$^+$ T cells against endogenous TRA antigens.

BMACs express Treg induction-associated genes and convert naïve T cells to Treg cells in vitro

To further evaluate the impact of BMACs on CD4$^+$ T cells through cognate interaction, we examined the expression of molecules that are essential signals for T cell activation or differentiation. As depicted in **Figure S5A**, BMACs strongly expressed the inhibitory checkpoint molecule PD-L1 (but weakly PD-L2) compared to other APC subsets in the BM, together with intermediate levels of CD80 and CD86, suggesting a mixed potential of promoting T cell tolerance and activation. Gene expression array analysis on *pc*-BMACs compared to BM plasma cells of Adig mice revealed that, in addition to significantly higher *Aire* expression, *pc*-BMACs displayed a distinct gene expression profile (**Figure S5B** and **S5C**). *pc*-BMACs selectively expressed genes, which are known to induce Treg generation or conversion, or to induce suppressive functions of Treg cells (Fig. 5A). For example, *pc*-BMACs differentially expressed genes for RA synthesis (*Aldh1a2* and *Rbp7*) (65, 66), as well as *Cd155* (also known as *Pvr*) which stimulates Treg upon ligation with TIGIT and subsequently enhances Treg-mediated suppression of cytotoxic T cell responses (69). *pc*-BMACs also showed a modest increase of *Semaphorin-4a* (*Sema4a*) expression, suggesting that they can promote the stability of Treg cells (70). In contrast, two other genes known to support Treg induction, *Tgfb1* and *Btla* (71)were expressed at lower levels in *pc*-BMACs than in plasma cells. Importantly, among the genes that were associated with tolerance induction, we observed an enrichment of genes associated with Treg induction, instead of genes related to general T-cell tolerance through ligating inhibitory receptors, as most of the ligands known for inhibitory receptors were downregulated, such as *Ceacam1*, *Lgals3* (also known as *Galectin-3*), *Arg1* (also known as *Arginase-1*) and *Ido1* (Fig. 5A). Similarly, *pc*-BMACs themselves did not exploit the tolerogenic mechanisms mediated by Treg cells. Notably, *pc*-BMACs showed *Il-10* and *LAG-3* expression, similar to the recently reported subset of natural regulatory plasma cells (72). However, *pc*-BMACs only express *ebi3* but not *p35* (also known as *Il-12a*), the subunits of IL-35, indicating that *pc*-BMACs employ distinct tolerogenic machineries than the regulatory plasma cells which mediate immune tolerance via IL-35 production (73). In line with the capacity of antigen presentation, *pc*-BMACs expressed higher

amounts of MHC-II and lysosomal proteases such as *asparaginyl endopeptidase* (*Lgmn*) and *cathepsins* that are essential for peptide processing and loading to MHC-II (74) (Fig. 5B). Together, our results demonstrate that *pc*-BMACs are equipped with antigen presentation capacity and multiple tolerance-associated machineries that are selective for inducing Treg cells.

We next exploited naïve $CD4^+$ T cells from HA-TCR transgenic mice (30)to assess the outcome of the engagement of cognate $CD4^+$ T cells to BMACs expressing Aire-regulated antigens. BMACs were sorted from Aire-HCO and Adig mice, and co-cultured with CD25-depleted naïve $CD4^+$ T cells from HA-TCR or WT Balb/c mice. After co-culture for 5 days, HA-specific $CD4^+$ T cells show upregulated CD25 and Foxp3 expression after encountering HA-expressing BMACs, indicating that BMACs induced a conversion of naïve $CD4^+$ T cells to Treg cells (Fig. 5C). In contrast, only less than 10% of their polyclonal counterpart showed CD25 upregulation. This induction was antigen-dependent, as BMACs from Adig mice did not induce the expression of CD25 and Foxp3 on HA-specific $CD4^+$ T cells. To further confirm that *pc*-BMACs among total BMACs are accountable for the induction of Treg cells, we sorted *pc*-BMACs as well as the rest of Aire-$hCD2^+$ cells (non-*pc*

-BMACs) to evaluate their abilities to induce Treg cells *in vitro*. As shown in Fig. 5D, the proportions of T cells converted to Treg cells after encountering *pc*-BMACs was comparable to total BMACs, while non-*pc*-BMACs showed lower capacity to induce Treg cells, indicating the tolerogenic capacity lies largely within *pc*-BMACs than in other $Aire^+$ cells in the BM. The induced Treg cells expressed LAP, suggesting their activated status after induction (**Figure S5D**). Of note, the induction of Treg cells by *pc*-BMACs was not dependent on TGFβ1, as anti-TGFβ1 neutralizing antibody did not affect Treg induction of naïve T cells after encountering *pc*-BMACs (**Figure S5E**).

BMACs induce bona fide Treg cells in vivo

To further assess the impact of BMACs on naïve $CD4^+$ T cells *in vivo*, we transferred CD25-depleted naïve HA-specific $CD4^+$ T cells along with polyclonal naïve $CD4^+$ T cells (as a reference population) into WT BM chimera mice, which were reconstituted with BM cells from Aire-HCO or WT mice 8 weeks prior to naïve T cell transfer. In the BM chimera mice, Aire-HA was expressed only in hematopoietic cells, thus avoiding the influence of HA expression by non-hematopoietic stromal cells. On day 3 post-transfer, HA-specific donor T cells showed robust proliferation in the BM of Aire-HCO hosts (**Figure S6A**). A comparable degree of proliferation of donor HA-specific T cells was neither observed in WT hosts, nor in Aire-HCO and WT hosts for polyclonal T cells, indicating that the expansion of the donor T cells was antigen-dependent. Of note, a substantial proportion of non-divided donor T cells were also found in BM, demonstrating the migration of naïve T cells into BM, as previously reported (7). Two weeks after T cell transfer, the frequency of HA-specific T cells remained more than two-fold of the polyclonal T cells in the BM, whereas in the spleen, less HA-specific T cells were detected than polyclonal ones (Fig. 6A, 6B and S6B). These results indicate antigen-specific activation of autoreactive T cells by BMACs in the BM. In accordance to the *in vitro* results, a much higher proportion of HA-specific T cells in the BM were

converted into $CD25^+Foxp3^+$ Treg cells (34.0 ± 6.5%) than in the spleen (10.9 ± 5.7%), as depicted in Fig. 6C, 6D, and S6C. The same effect was not observed in polyclonal T cells in Aire-HCO host, nor in HA-specific T cells in WT host, indicating that the conversion of Treg cells depends on the cognate antigens presented by BMACs. To verify the stability of BMAC-induced Treg cells, we sorted the HA-specific Treg cells induced by BMACs (BMAC-Tregs) and the $CD25^-Foxp3^-$ HA-specific T cells (donor Tconvs) at 14 days post transfer, and conducted bisulfite sequencing to assess the methylation status of the Treg-specific demethylated region (TSDR) in the *Foxp3* gene. In addition, we measured epigenetic modification of Treg-specific signature genes such as *Il2ra*, *Ctla4*, *Tnfrsf18* (encoding GITR), and *Ikzf2* (encoding Helios) (49, 75, 76). As shown in Fig. 6E, 6F and S6D, BMAC-Tregs showed significantly lower levels of methylation at *Foxp3*, *Il2ra*, *Ctla4* and *Tnfrsf18* loci compared to donor Tconvs as well as iTregs induced *in vitro* by TGFβ1 (*in vitro* iTreg). There was no significant difference of the methylation status at these loci among BMAC-Tregs, host pTregs and tTregs, indicating that BMAC-Tregs undergo profound epigenetic changes and acquire lineage stability marks of Treg cells. At *Ikzf2* locus, BMAC-Tregs displayed similar levels of methylation as host pTregs, suggesting a signature of peripheral induction of BMAC-Tregs (Fig. 6E and 6F). Consistent to the methylation status, the accessibilities of chromatin regions at *Foxp3*, *Il2ra*, *Ctla4*, and *Tnfrsf18* of BMAC-Tregs acquired by ATAC-seq are comparable to those of host tTregs and pTregs (**Figure S6E**). More importantly, PCA and unsupervised clustering of genome-wide accessible chromatin regions revealed that BMAC-Tregs display the chromatin profiles similar to host Tregs (most similar to pTregs), but different to Tconvs and *in vitro* iTregs (Fig. 6G and **H**). Of note, BMAC-Tregs also show open chromatin at *Tgfb1* locus (data not shown). In addition, up to 18.4% of BM Treg cells showed pTreg phenotype ($Helios^-$), indicating a substantial proportion of BM Treg cells are peripherally induced (**Figure S6F**). These data show that BMACs induce the conversion of naïve T cells that recognize Aire-regulated antigens into *bona fide* Treg cells *in vivo*.

We sought to determine whether the BMAC-induced Treg cells are functional in terms of immune suppression. In Aire-HCO hosts, we observed that the BMAC-induced Treg cells significantly upregulated the expression of CTLA-4 and LAP, but not of LAG-3, compared to the ones in WT host (Fig. 7A), indicating an activated and functional status of these Treg cells after recognizing the cognate antigens presented by BMACs (77, 78). Such activation status was found only for minor fractions of HA-specific donor cells in the spleen (**Figure S7A**). To evaluate the suppressive function of BMAC-Tregs, we sorted HA-specific Tregs induced by BMACs after 14 days post transfer and test their suppressive capacity *ex vivo*. To this end, they were co-cultured with CFSE-labeled responder naïve $CD4^+$ T cells in the presence of CD3/CD28 stimulation. As shown in Fig. 7B, both BMAC-Tregs and host Tregs suppressed the proliferation of responder cells to a similar degree in a dose-dependent manner, indicating similar suppressive function of BMAC-Tregs to that of host Tregs. We next assessed, whether BMAC-induced Treg cells are capable to regulate cytotoxic T cell responses *in vivo*. After naïve HA-specific $CD4^+$ T cells were converted into Treg cells in Aire-HCO hosts, we injected HA peptide-pulsed $CFSE^{high}$ and non-pulsed $CFSE^{low}$ target cells, together with or without cytotoxic HA-specific effector T cells isolated from the BM and spleen of WT mice immunized with HA peptide. One day after the transfer of target cells and cytotoxic effector T cells, we analyzed the frequencies of remaining $B220^+$ CFSE-labeled cells in the BM

or spleen of Aire-HCO or WT hosts. As depicted in Fig. 7C, compared to WT hosts, HA-specific cytotoxicity in the BM was reduced in the Aire-HCO hosts, in which HA-specific $CD4^+$ T cells were converted into Treg cells. No significant suppressive effect was observed in the spleen, reflecting the lack of activation status of the induced Treg cells in the spleen (Fig. 7C and S7B). Taken together, these data indicate that BMAC-induced Treg cells are activated and functionally competent.

Discussion

We here report a subset of Aire-expressing antigen presenting cells – *pc*-BMACs – that induces in the BM the generation of *bona fide* Treg which show demethylated *Foxp3* TSDR and other loci of Treg-related genes such as *Il2ra*, *Ctla4* and *Gitr*, indicating their epigenetic fixation towards a stable Treg lineage (76). Indeed, we found that *pc*-BMAC-induced pTregs showed comparable capacity as tTregs and host-derived pTregs in suppressing T cell proliferation. Furthermore, *pc*-BMAC-induced Treg cells unambiguously displayed an activated status indicated by expression of LAP which suggests a constant TCR trigger by BMAC expressed antigens.

Genetic mouse models selectively lacking pTregs showed that this subset plays critical roles in maintaining oral tolerance and particularly in preventing the onset of severe autoimmune diseases (79–83). Therefore, this Treg subset represents an important part of the entire Treg repertoire, which makes up about 15% to 30% of Treg cells in secondary lymphoid organs including LNs and spleen, and in the blood (84, 85). Oral tolerance is induced in the gut by generation of pTregs from naïve T cells specific for foreign antigens such as commensal bacteria and food antigens. This occurs under specific $TGF\beta^{high}RA^{high}$, tolerogenic microenvironmental conditions characteristic for the gut mucosa by local $CD103^+$ dendritic cells which acquire these antigens from the environment in the Peyer's patches and present them to naïve $CD4^+$ T cells in mesenteric LNs (86, 87). In contrast, pTregs that prevent the onset of autoimmune diseases such as multiple sclerosis and type 1 diabetes, similar to tTregs, need to recognize tissue restricted self-antigens such as MOG (81) or insulin (82). So far, the mechanism of their physiological induction in the periphery remains elusive.

Using single cell RNA-seq in nearly 200 single *pc*-BMACs, we here demonstrate that *pc*-BMACs in the BM promiscuously express more than 2000 tissue-restricted antigens covering a broad spectrum of peripheral tissues and that they can present them via MHC-II to naïve $CD4^+$ T cells. It is thus conceivable, that *pc*-BMACs, by inducing the conversion of self-reactive naïve $CD4^+$ T cells into pTregs, can contribute to peripheral tolerance towards most tissues of the body. Altogether, TRAs expressed by *pc*-BMACs made up half of the TRAs described (57). While the spectrum of TRAs expressed by *pc*-BMACs largely overlapped with that of mTECs, the role of Aire as a driver of TRA expression was less obvious in *pc*-BMACs compared to mTECs. In mTECs about 2300 TRAs are expressed in an Aire-dependent manner (61), but only 210 of these Aire-dependent TRAs were expressed in *pc*-BMACs, potentially resulting from the lower expression level of Aire in BMACs. Thus, *pc*-BMACs largely cover the Aire-independent repertoire of TRAs in mTECs. Still, upon comparison with *pc*-BMACs from Aire-deficient mice we found a

significant impact of Aire on the expression of several TRAs but on the other hand the vast majority of TRAs expressed by *pc*-BMACs was not regulated by Aire. The relevance of Aire for TRA expression has been largely established by studies with mTECs but even in mTECs many TRAs can be expressed independently of Aire. Thus, while Aire can drive TRA expression in mTECs, it may not always be required for this purpose in other cell types or circumstances. This raises the question, whether in *pc*-BMACs Aire might take over other functions. In this regard, it is noteworthy that in *pc*-BMACs Aire controlled the expression of more than 100 genes which were not TRAs. Interestingly, several genes playing instrumental roles in Treg induction including *Icosl* and RA synthesis-related genes such as *Aldh1a2* and *Aldh1b1* were strictly Aire-dependent in *pc*-BMACs. This points to the possibility that apart from TRA expression, Aire regulates tolerogenic functions in antigen presenting cells and plays a functional role in Treg induction in the BM. This might occur in synergy with *Il-10* and the TIGIT ligand *Cd155* which were overexpressed in *pc*-BMACs compared to classical plasma cells. Notably, BMACs express many tolerance-inducing genes associated with tolerogenic DCs, such as *Il-10*, *Ebi3*, and aldehyde dehydrogenases associated with RA synthesis (88). However, Treg induction by *pc*-BMAC, in contrast to that by tolerogenic DCs in the gut, was independent of TGFβ1. Indeed, a recent study reported a role of Aire in suppressing B cell activating capacities of dendritic cells (88). Altogether, we thus report here a novel cell subset capable of inducing pTregs against self-antigens in the BM in which Aire might play a tolerogenic role beyond controlling TRA expression.

The BM is a known main reservoir of Treg cells (10) and as such a major site for the regulation and maintenance of local and systemic tolerance. While extensive recirculation of Treg from and to the BM has been described, a potential contribution of BM intrinsic mechanisms to generate a repertoire of self-reactive Treg has not been addressed so far. Our finding provides insight into the regulation of active T cell tolerance: under physiological conditions, both immigrant and *in situ*-generated autoreactive Treg cells may contribute to the diverse Treg repertoire in the BM. These regulatory cells assist the homeostasis of hematopoiesis by modulating the differentiation of hematopoietic stem cells and providing immune-privileged niches (11, 13). At the onset of inflammation in the periphery, these autoreactive Treg cells, upon activation, migrate from the BM to inflammatory sites and regulate local inflammation (9, 10, 16). The TRAs expressed by BMACs included self-antigens associated to autoimmune diseases and cancers, indicating that BMACs can induce Treg cells that are specific to these self-antigens and important for controlling autoimmune diseases or for promoting tumor growth. It is noteworthy that although our data showed *pc*-BMACs alone can induce the conversion of Treg cells in vitro, we do not exclude the possibility that in vivo other APC subsets can acquire the antigens from *pc*-BMACs and further induce T cell tolerance. In addition to inducing pTregs, it is possible that *pc*-BMACs contribute to the maintenance of self-tolerance by supporting the survival of tTregs in the BM (89), as the majority of TRAs expressed by BMACs is shared with mTECs in the thymus.

Recent evidences showed that self-representation by lymph node stromal cells contributes to the maintenance of T cell tolerance through pGE (90, 89). While lymph node stromal cells support Treg cell homeostasis (91), a role in Treg induction has not been described for these subsets. Likewise, another subset of TRA expressing cells, eTACs, induces anergy of autoreactive $CD4^+$ T cells in peripheral

lymphoid organs (22, 23). Of note, the tolerogenic capacity of eTACs lies in inactivating $CD4^+$ T cells through the absence of costimulatory molecules rather than inducing functional Treg cells. Another $Aire^+Rorc^+$ APC subset in the LNs was originally classified as ILC3-like cells (26), but later reclassified as Janus cells (24) due to their similarity to migratory DCs. These cells can efficiently present endogenous antigens to $CD4^+$ and $CD8^+$ T cells and are involved in deletion of autoreactive $CD4^+$ and $CD8^+$ T cells in secondary lymphoid organs, though not in Treg induction (26, 24). A second subset of RORγt-dependent $Aire^+$ APCs, termed Thetis cells, was found in lymph nodes during early life and is transcriptionally distinct from ILC3-like/Janus cells (25). Thetis cells mediate immune tolerance by induction of peripheral Tregs in lymph nodes of juvenile mice (max. 3 weeks), most likely via the TGFβ pathway. It is noteworthy that HA-specific donor $CD4^+$ T cells in the spleen diminished compared to their polyclonal counterparts 2 weeks after being transferred into hosts with Aire-HA hematopoietic cells, in agreement with the deletional effect of eTACs and ILC3-like $Aire^+$ cells (22, 26). In contrast, BMAC-induced Treg cells are independent of TGFβ1 and maintained high frequencies for at least 2 weeks. These findings suggest that *pc*-BMACs exploit different tolerogenic mechanisms to control autoreactive $CD4^+$ T cells. Recently, the landscape of extrathymic $Aire^+$ APCs has been summarized by Sun *et al.* (2025) (27), suggesting the reclassification of ILC3-like $Aire^+$ cells (26), Janus cells (24), eTACs (28), and Thetis cells (25) to the unified nomenclature of RORγt-eTAC subset 1–3 (27). However, the myeloid lineage of RORγt-eTACs as well as their specific functionality distinguishes them from the lymphoid *pc*-BMACs we describe here. Specifically, cell numbers of RORγt-eTACs, are unaffected by *Rag2* and *Il2rg*-knockout, whereas *pc*-BMACs are strongly dependent on *Rag2*. The *Rag2*-independent BM Aire-expressing cells show no characteristics of plasma cells, and the non-plasma cell-like counterpart of BM $Aire^+$ cells do not induce Treg conversion *in vitro*. However, it requires further studies to determine whether the *Rag2*-independent Aire-expressing cells belong to the any of the RORγt-eTAC subsets. A detailed comparison of the gene signatures published in the scRNA-seq dataset characterizing RORγt-eTAC subset 1–3 (GSE273746 & GSE285182) and the gene signature we describe for *pc*-BMACs (GSE136650) emphasizes the differences between these cell subsets. For example, RORγt-eTAC1 are defined as EpCAM-negative which marks them distinct from the $EpCAM^+$ *pc*-BMACs. RORγt-eTAC 1–3 are defined by expression of *Rorc*, but lack *Prdm1*. However, *pc*-BMACs are distinguished by Blimp-1 (*Prdm1*) expression and do not express *Rorc*, further delineating the differences in subset identity. Sun et al. (2025) list *Prdm16, Il4i1, Thrb, and Ube2e2* as key markers for RORγt-eTACs, all of which are not expressed in *pc*-BMACs. Thus, we conclude that BMACs are a phenotypically and functionally distinct subset of Aire-expressing APCs. Nevertheless, our data do not exclude the possibility that Treg cells could also be induced elsewhere by hitherto unidentified Aire-expressing cells and then migrate into the BM.

Using Adig mice for phenotypic analysis of *pc*-BMACs, we demonstrate that they express EpCAM and low levels of MHC-II, and Aire-expressing cells in human showed the same $EpCAM^+HLA\text{-}DR^{low}$ phenotype, suggesting this cell population is present in both species. Moreover, we detected Aire protein expression in both WT mice and human using intracellular staining and flow cytometric analysis, and found indication of nuclear expression pattern of Aire protein in WT mice using immunofluorescent

tissue staining, despite we did not further quantify GFP and Aire protein co-expression in the BM of Adig mice. *pc*-BMACs displayed a $CD19^{low}CD138^{+}B220^{-}Blimp\text{-}1^{+}$ plasma cell-like phenotype, which indicates that the B cell lineage is not only involved in promoting negative selection of T cells in the thymus (29), but also in the maintenance of peripheral T cell tolerance in the BM. In Adig mice, approximately half of the thymic B cells are Aire-GFP^{+} (that is about 0.05% of total thymic cells). In hind bones of 6–12 weeks old mice, BMACs make up a comparable proportion (0.01%-0.04%) of total BM cells. Despite the scarceness of these cell subsets, they contribute to central and peripheral T cell tolerance, respectively. Isotype analyses have revealed that Aire-expressing thymic B cells contain $IgM^{+}IgD^{+}$ and $IgM^{+}IgD^{-}$ cells, as well as $IgM^{-}IgD^{-}$ cells which undergo class switch after CD40-licensing (29). Unlike in thymic B cells, the majority of BMACs were surface IgM^{+}, indicating that class switch is not coupled with Aire expression in the BM. Noteably, although Sca-1 expression has been reported on plasma cells (52), it is unclear whether the expression of Sca-1 on BMACs indicates their early stage of hematopoietic stem cell development. The licensing of thymic B cells requires the cognate interaction via peptide:MHC-II and TCR between B cells and cognate $CD4^{+}$ T cells, which provide a CD40 signal to induce Aire, MHC-II and ectopic TRA expression. Whether the interaction with $CD4^{+}$ T cells and CD40 signaling is essential for *pc*-BMACs to express Aire should be further assessed.

In conclusion, our results unravel for the first time a direct conversion of naïve $CD4^{+}$ T cells into functional, self-antigen reactive Treg cells outside the thymus by a BM-resident population of $Aire^{+}$ cells capable of pGE. This mechanism contributes to the formation of the repertoire of pTregs in the BM that mediates local and systemic peripheral tolerance against tissue-restricted self-antigens.

Declarations

Conflict of Interest

M.D. received personal fees from Odyssey Therapeutics outside the submitted work.

Supplementary Information

Supplementary items are available at *CMI's* Websit

Author contributions

C.-Y.C., F.K., B.K. and P.B. designed the study; C.-Y.C., F.K., S.-H.W., F.D., S.P., T.Y., M.De., C.S. and P.B. designed experiments; C.-Y.C., F.K., F.D., S.P., T.Y., D.R., M.De., M.G., C.G., G.W., V.V. and A.N.M. performed experiments; C.-Y.C., F.K., S.-H.W., F.D., M.De., M.Di., C.D.I., A.M., R.K., M.G., C.S., AW and B.B. analyzed data; P.P. and M.S.A. and developed mouse models; S.P., T.Y., M.De., Y.S., P.P., M.R., S.S., M.X., C.A.K.,

M.S.A., C.S., M.F., B.B. and B.K. advised on techniques and methodology; S.P., P.P., M.R., C.A.K., M.S.A. C.S., M.F. and AW contributed to manuscript preparation; C.-Y.C. and P.B. wrote the manuscript.

Correspondence to Philipp Beckhove

Acknowledgements

We thank R. Eder and I. Fink in the RCI Cell Sorting and Analysis Core Facility for bulk and single cell sorting, the RCI Genomics Core Facility for sequencing services of libraries from bulk RNA-seq, ATAC-seq, and bisulfite-seq, and Biomedical Sequencing Facility (BSF) at the Research Center for Molecular Medicine (CeMM) of the Austrian Academy of Sciences for single cell RNA-seq service. We also would like to thank K. Hexel and S. Schmitt in DKFZ Flow Cytometry Core Facility for single cell sorting, the Microarrys Unit in Genomics and Proteomics Core Facility in DKFZ for providing the Illumina Expression Beadchips and Omics IT and Data Management Core Facility (ODCF) in DKFZ for aligning sequencing data. We further thank Prof. L. Klein from the Institute for Immunology at Ludwig-Maximilians-University, Munich for providing Aire-HCO mice and initial discussions. This work is supported by DFG (KL 1233/10 – 2 for C.A.K. and FOR127; BE 2610/6 – 1 for P.B). The authors declare no competing financial interests.

References

1. Mercier FE, Ragu C, Scadden DT. The bone marrow at the crossroads of blood and immunity. Nat Rev Immunol 2011; 12:49–60.
2. Tokoyoda K, Hauser AE, Nakayama T, Radbruch A. Organization of immunological memory by bone marrow stroma. Nat Rev Immunol 2010; 10:193–200.
3. Choi C, Witzens M, Bucur M, Feuerer M, Sommerfeldt N, Trojan A et al. Enrichment of functional CD8 memory T cells specific for MUC1 in bone marrow of patients with multiple myeloma. Blood 2005; 105:2132–4.
4. Müller-Berghaus J, Ehlert K, Ugurel S, Umansky V, Bucur M, Schirrmacher V et al. Melanoma-reactive T cells in the bone marrow of melanoma patients: association with disease stage and disease duration. Cancer Res 2006; 66:5997–6001.
5. Domschke C, Ge Y, Bernhardt I, Schott S, Keim S, Juenger S et al. Long-term survival after adoptive bone marrow T cell therapy of advanced metastasized breast cancer: follow-up analysis of a clinical pilot trial. Cancer Immunol Immunother 2013; 62:1053–60.
6. Feuerer M, Beckhove P, Bai L, Solomayer EF, Bastert G, Diel IJ et al. Therapy of human tumors in NOD/SCID mice with patient-derived reactivated memory T cells from bone marrow. Nat Med 2001; 7:452–8.
7. Feuerer M, Beckhove P, Garbi N, Mahnke Y, Limmer A, Hommel M et al. Bone marrow as a priming site for T-cell responses to blood-borne antigen. Nat Med 2003; 9:1151–7.

8. Tripp RA, Topham DJ, Watson SR, Doherty PC. Bone marrow can function as a lymphoid organ during a primary immune response under conditions of disrupted lymphocyte trafficking. J Immunol 1997; 158:3716–20.
9. Zhao E, Xu H, Wang L, Kryczek I, Wu K, Hu Y et al. Bone marrow and the control of immunity. Cell Mol Immunol 2012; 9:11–9.
10. Zou L, Barnett B, Safah H, Larussa VF, Evdemon-Hogan M, Mottram P et al. Bone marrow is a reservoir for CD4 + CD25+ regulatory T cells that traffic through CXCL12/CXCR4 signals. Cancer Res 2004; 64:8451–5.
11. Fujisaki J, Wu J, Carlson AL, Silberstein L, Putheti P, Larocca R et al. In vivo imaging of Treg cells providing immune privilege to the haematopoietic stem-cell niche. Nature 2011; 474:216–9.
12. Pierini A, Nishikii H, Baker J, Kimura T, Kwon H-S, Pan Y et al. Foxp3 + regulatory T cells maintain the bone marrow microenvironment for B cell lymphopoiesis. Nat Commun 2017; 8:15068.
13. Urbieta M, Barao I, Jones M, Jurecic R, Panoskaltsis-Mortari A, Blazar BR et al. Hematopoietic progenitor cell regulation by CD4 + CD25+ T cells. Blood 2010; 115:4934–43.
14. Le Texier L, Lineburg KE, MacDonald KPA. Harnessing bone marrow resident regulatory T cells to improve allogeneic stem cell transplant outcomes. Int J Hematol 2017; 105:153–61.
15. Schmidt H-H, Ge Y, Hartmann FJ, Conrad H, Klug F, Nittel S et al. HLA Class II tetramers reveal tissue-specific regulatory T cells that suppress T-cell responses in breast carcinoma patients. Oncoimmunology 2013; 2:e24962.
16. Rathinasamy A, Domschke C, Ge Y, Böhm H-H, Dettling S, Jansen D et al. Tumor specific regulatory T cells in the bone marrow of breast cancer patients selectively upregulate the emigration receptor S1P1. Cancer Immunol Immunother 2017; 66:593–603.
17. Wei S, Kryczek I, Zou W. Regulatory T-cell compartmentalization and trafficking. Blood 2006; 108:426–31.
18. Derbinski J, Schulte A, Kyewski B, Klein L. Promiscuous gene expression in medullary thymic epithelial cells mirrors the peripheral self. Nat Immunol 2001; 2:1032–9.
19. Klein L, Kyewski B, Allen PM, Hogquist KA. Positive and negative selection of the T cell repertoire: what thymocytes see (and don't see). Nat Rev Immunol 2014; 14:377–91.
20. Anderson MS, Venanzi ES, Klein L, Chen Z, Berzins SP, Turley SJ et al. Projection of an immunological self shadow within the thymus by the aire protein. Science 2002; 298:1395–401.
21. Mathis D, Benoist C. Aire. Annu Rev Immunol 2009; 27:287–312.
22. Gardner JM, Devoss JJ, Friedman RS, Wong DJ, Tan YX, Zhou X et al. Deletional tolerance mediated by extrathymic Aire-expressing cells. Science 2008; 321:843–7.
23. Gardner JM, Metzger TC, McMahon EJ, Au-Yeung BB, Krawisz AK, Lu W et al. Extrathymic Aire-expressing cells are a distinct bone marrow-derived population that induce functional inactivation of $CD4^+$ T cells. Immunity 2013; 39:560–72.

24. Wang J, Lareau CA, Bautista JL, Gupta AR, Sandor K, Germino J et al. Single-cell multiomics defines tolerogenic extrathymic Aire-expressing populations with unique homology to thymic epithelium. Sci Immunol 2021; 6:eabl5053.
25. Akagbosu B, Tayyebi Z, Shibu G, Paucar Iza YA, Deep D, Parisotto YF et al. Novel antigen-presenting cell imparts Treg-dependent tolerance to gut microbiota. Nature 2022; 610:752–60.
26. Yamano T, Dobeš J, Vobořil M, Steinert M, Brabec T, Ziętara N et al. Aire-expressing ILC3-like cells in the lymph node display potent APC features. J Exp Med 2019; 216:1027–37.
27. Sun I-H, Qualls AE, Yin HS, Wang J, Arvedson MP, Germino J et al. RORγt eTACs mediate oral tolerance and Treg induction. J Exp Med 2025; 222.
28. Abramson J, Dobeš J, Lyu M, Sonnenberg GF. The emerging family of RORγt+ antigen-presenting cells. Nat Rev Immunol 2024; 24:64–77.
29. Yamano T, Nedjic J, Hinterberger M, Steinert M, Koser S, Pinto S et al. Thymic B Cells Are Licensed to Present Self Antigens for Central T Cell Tolerance Induction. Immunity 2015; 42:1048–61.
30. Aschenbrenner K, D'Cruz LM, Vollmann EH, Hinterberger M, Emmerich J, Swee LK et al. Selection of Foxp3 + regulatory T cells specific for self antigen expressed and presented by Aire+ medullary thymic epithelial cells. Nat Immunol 2007; 8:351–8.
31. Hubert F-X, Kinkel SA, Crewther PE, Cannon PZF, Webster KE, Link M et al. Aire-deficient C57BL/6 mice mimicking the common human 13-base pair deletion mutation present with only a mild autoimmune phenotype. J Immunol 2009; 182:3902–18.
32. Muranski P, Boni A, Antony PA, Cassard L, Irvine KR, Kaiser A et al. Tumor-specific Th17-polarized cells eradicate large established melanoma. Blood 2008; 112:362–73.
33. Brennecke P, Reyes A, Pinto S, Rattay K, Nguyen M, Küchler R et al. Single-cell transcriptome analysis reveals coordinated ectopic gene-expression patterns in medullary thymic epithelial cells. Nat Immunol 2015; 16:933–41.
34. Liiv I, Rebane A, Org T, Saare M, Maslovskaja J, Kisand K et al. DNA-PK contributes to the phosphorylation of AIRE: importance in transcriptional activity. Biochim Biophys Acta 2008; 1783:74–83.
35. Corces MR, Trevino AE, Hamilton EG, Greenside PG, Sinnott-Armstrong NA, Vesuna S et al. An improved ATAC-seq protocol reduces background and enables interrogation of frozen tissues. Nat Methods 2017; 14:959–62.
36. Jiang H, Lei R, Ding S-W, Zhu S. Skewer: a fast and accurate adapter trimmer for next-generation sequencing paired-end reads. BMC Bioinformatics 2014; 15:182.
37. Langmead B, Salzberg SL. Fast gapped-read alignment with Bowtie 2. Nat Methods 2012; 9:357–9.
38. Tarasov A, Vilella AJ, Cuppen E, Nijman IJ, Prins P. Sambamba: fast processing of NGS alignment formats. Bioinformatics 2015; 31:2032–4.
39. Quinlan AR, Hall IM. BEDTools: a flexible suite of utilities for comparing genomic features. Bioinformatics 2010; 26:841–2.

40. Heinz S, Benner C, Spann N, Bertolino E, Lin YC, Laslo P et al. Simple combinations of lineage-determining transcription factors prime cis-regulatory elements required for macrophage and B cell identities. Mol Cell 2010; 38:576–89.
41. An integrated encyclopedia of DNA elements in the human genome. Nature 2012; 489:57–74.
42. Hansen KD, Irizarry RA, Wu Z. Removing technical variability in RNA-seq data using conditional quantile normalization. Biostatistics 2012; 13:204–16.
43. Love MI, Huber W, Anders S. Moderated estimation of fold change and dispersion for RNA-seq data with DESeq2. Genome Biol 2014; 15:550.
44. Dafforn A, Chen P, Deng G, Herrler M, Iglehart D, Koritala S et al. Linear mRNA amplification from as little as 5 ng total RNA for global gene expression analysis. Biotechniques 2004; 37:854–7.
45. Reisinger E, Genthner L, Kerssemakers J, Kensche P, Borufka S, Jugold A et al. OTP: An automatized system for managing and processing NGS data. J Biotechnol 2017; 261:53–62.
46. Picelli S, Faridani OR, Björklund AK, Winberg G, Sagasser S, Sandberg R. Full-length RNA-seq from single cells using Smart-seq2. Nat Protoc 2014; 9:171–81.
47. Bot A, Bot S, Antohi S, Karjalainen K, Bona C. Kinetics of generation and persistence on membrane class II molecules of a viral peptide expressed on foreign and self proteins. J Immunol 1996; 157:3436–42.
48. Quah BJC, Warren HS, Parish CR. Monitoring lymphocyte proliferation in vitro and in vivo with the intracellular fluorescent dye carboxyfluorescein diacetate succinimidyl ester. Nat Protoc 2007; 2:2049–56.
49. Delacher M, Imbusch CD, Weichenhan D, Breiling A, Hotz-Wagenblatt A, Träger U et al. Genome-wide DNA-methylation landscape defines specialization of regulatory T cells in tissues. Nat Immunol 2017; 18:1160–72.
50. Su MA, Giang K, Zumer K, Jiang H, Oven I, Rinn JL et al. Mechanisms of an autoimmunity syndrome in mice caused by a dominant mutation in Aire. J Clin Invest 2008; 118:1712–26.
51. Blanc P, Moro-Sibilot L, Barthly L, Jagot F, This S, Bernard S de et al. Mature IgM-expressing plasma cells sense antigen and develop competence for cytokine production upon antigenic challenge. Nat Commun 2016; 7:13600.
52. Wilmore JR, Jones DD, Allman D. Protocol for improved resolution of plasma cell subpopulations by flow cytometry. Eur J Immunol 2017; 47:1386–8.
53. Todd DJ, McHeyzer-Williams LJ, Kowal C, Lee A-H, Volpe BT, Diamond B et al. XBP1 governs late events in plasma cell differentiation and is not required for antigen-specific memory B cell development. J Exp Med 2009; 206:2151–9.
54. Minnich M, Tagoh H, Bönelt P, Axelsson E, Fischer M, Cebolla B et al. Multifunctional role of the transcription factor Blimp-1 in coordinating plasma cell differentiation. Nat Immunol 2016; 17:331–43.

55. Miller JJ, Cole LJ. The radiation resistance of long-lived lymphocytes and plasma cells in mouse and rat lymph nodes. J Immunol 1967; 98:982–90.
56. Anderson MS, Su MA. AIRE expands: new roles in immune tolerance and beyond. Nat Rev Immunol 2016; 16:247–58.
57. Derbinski J, Gäbler J, Brors B, Tierling S, Jonnakuty S, Hergenhahn M et al. Promiscuous gene expression in thymic epithelial cells is regulated at multiple levels. J Exp Med 2005; 202:33–45.
58. Kyewski B, Derbinski J. Self-representation in the thymus: an extended view. Nat Rev Immunol 2004; 4:688–98.
59. Walsh MJ, Murray JM. Dual implication of 2',3'-cyclic nucleotide 3' phosphodiesterase as major autoantigen and C3 complement-binding protein in the pathogenesis of multiple sclerosis. J Clin Invest 1998; 101:1923–31.
60. Dart ML, Jankowska-Gan E, Huang G, Roenneburg DA, Keller MR, Torrealba JR et al. Interleukin-17-dependent autoimmunity to collagen type V in atherosclerosis. Circ Res 2010; 107:1106–16.
61. Sansom SN, Shikama-Dorn N, Zhanybekova S, Nusspaumer G, Macaulay IC, Deadman ME et al. Population and single-cell genomics reveal the Aire dependency, relief from Polycomb silencing, and distribution of self-antigen expression in thymic epithelia. Genome Res 2014; 24:1918–31.
62. Pinto S, Michel C, Schmidt-Glenewinkel H, Harder N, Rohr K, Wild S et al. Overlapping gene coexpression patterns in human medullary thymic epithelial cells generate self-antigen diversity. Proc Natl Acad Sci U S A 2013; 110:E3497-505.
63. Akbari O, Freeman GJ, Meyer EH, Greenfield EA, Chang TT, Sharpe AH et al. Antigen-specific regulatory T cells develop via the ICOS-ICOS-ligand pathway and inhibit allergen-induced airway hyperreactivity. Nat Med 2002; 8:1024–32.
64. Lee H-J, Kim S-N, Jeon M-S, Yi T, Song SU. ICOSL expression in human bone marrow-derived mesenchymal stem cells promotes induction of regulatory T cells. Sci Rep 2017; 7:44486.
65. Benson MJ, Pino-Lagos K, Rosemblatt M, Noelle RJ. All-trans retinoic acid mediates enhanced T reg cell growth, differentiation, and gut homing in the face of high levels of co-stimulation. J Exp Med 2007; 204:1765–74.
66. Kedishvili NY. Retinoic Acid Synthesis and Degradation. Subcell Biochem 2016; 81:127–61.
67. Vogt AB, Spindeldreher S, Kropshofer H. Clustering of MHC-peptide complexes prior to their engagement in the immunological synapse: lipid raft and tetraspan microdomains. Immunol Rev 2002; 189:136–51.
68. Messele T, Roos MT, Hamann D, Koot M, Fontanet AL, Miedema F et al. Nonradioactive techniques for measurement of in vitro T-cell proliferation: alternatives to the (3)Hthymidine incorporation assay. Clin Diagn Lab Immunol 2000; 7:687–92.
69. Joller N, Lozano E, Burkett PR, Patel B, Xiao S, Zhu C et al. Treg cells expressing the coinhibitory molecule TIGIT selectively inhibit proinflammatory Th1 and Th17 cell responses. Immunity 2014; 40:569–81.

70. Delgoffe GM, Woo S-R, Turnis ME, Gravano DM, Guy C, Overacre AE et al. Stability and function of regulatory T cells is maintained by a neuropilin-1-semaphorin-4a axis. Nature 2013; 501:252–6.
71. Jones A, Bourque J, Kuehm L, Opejin A, Teague RM, Gross C et al. Immunomodulatory Functions of BTLA and HVEM Govern Induction of Extrathymic Regulatory T Cells and Tolerance by Dendritic Cells. Immunity 2016; 45:1066–77.
72. Lino AC, van Dang D, Lampropoulou V, Welle A, Joedicke J, Pohar J et al. LAG-3 Inhibitory Receptor Expression Identifies Immunosuppressive Natural Regulatory Plasma Cells. Immunity 2018; 49:120–133.e9.
73. Shen P, Roch T, Lampropoulou V, O'Connor RA, Stervbo U, Hilgenberg E et al. IL-35-producing B cells are critical regulators of immunity during autoimmune and infectious diseases. Nature 2014; 507:366–70.
74. Roche PA, Furuta K. The ins and outs of MHC class II-mediated antigen processing and presentation. Nat Rev Immunol 2015; 15:203–16.
75. Huehn J, Polansky JK, Hamann A. Epigenetic control of FOXP3 expression: the key to a stable regulatory T-cell lineage? Nat Rev Immunol 2009; 9:83–9.
76. Morikawa H, Sakaguchi S. Genetic and epigenetic basis of Treg cell development and function: from a FoxP3-centered view to an epigenome-defined view of natural Treg cells. Immunol Rev 2014; 259:192–205.
77. Sakaguchi S, Wing K, Onishi Y, Prieto-Martin P, Yamaguchi T. Regulatory T cells: how do they suppress immune responses? Int Immunol 2009; 21:1105–11.
78. Vignali DAA, Collison LW, Workman CJ. How regulatory T cells work. Nat Rev Immunol 2008; 8:523–32.
79. Bilate AM, Lafaille JJ. Induced CD4 + Foxp3+ regulatory T cells in immune tolerance. Annual review of immunology 2012; 30:733–58. Available from: URL: https://pubmed.ncbi.nlm.nih.gov/22224762/.
80. Campbell C, Dikiy S, Bhattarai SK, Chinen T, Matheis F, Calafiore M et al. Extrathymically Generated Regulatory T Cells Establish a Niche for Intestinal Border-Dwelling Bacteria and Affect Physiologic Metabolite Balance. Immunity 2018; 48:1245–1257.e9.
81. Jones A, Hawiger D. Peripherally Induced Regulatory T Cells: Recruited Protectors of the Central Nervous System against Autoimmune Neuroinflammation. Front. Immunol. 2017; 8:532.
82. Schuster C, Jonas F, Zhao F, Kissler S. Peripherally induced regulatory T cells contribute to the control of autoimmune diabetes in the NOD mouse model. Eur J Immunol 2018; 48:1211–6.
83. Yadav M, Stephan S, Bluestone JA. Peripherally induced tregs - role in immune homeostasis and autoimmunity. Front. Immunol. 2013; 4:232.
84. Thornton AM, Korty PE, Tran DQ, Wohlfert EA, Murray PE, Belkaid Y et al. Expression of Helios, an Ikaros transcription factor family member, differentiates thymic-derived from peripherally induced Foxp3 + T regulatory cells. J Immunol 2010; 184:3433–41.

85. Haribhai D, Williams JB, Jia S, Nickerson D, Schmitt EG, Edwards B et al. A requisite role for induced regulatory T cells in tolerance based on expanding antigen receptor diversity. Immunity 2011; 35:109–22.
86. Coombes JL, Siddiqui KRR, Arancibia-Cárcamo CV, Hall J, Sun C-M, Belkaid Y et al. A functionally specialized population of mucosal CD103 + DCs induces Foxp3 + regulatory T cells via a TGF-beta and retinoic acid-dependent mechanism. J Exp Med 2007; 204:1757–64.
87. Kim KS, Hong S-W, Han D, Yi J, Jung J, Yang B-G et al. Dietary antigens limit mucosal immunity by inducing regulatory T cells in the small intestine. Science 2016; 351:858–63.
88. Lindh E, Lind SM, Lindmark E, Hässler S, Perheentupa J, Peltonen L et al. AIRE regulates T-cell-independent B-cell responses through BAFF. Proc Natl Acad Sci U S A 2008; 105:18466–71.
89. Humbert M, Hugues S, Dubrot J. Shaping of Peripheral T Cell Responses by Lymphatic Endothelial Cells. Front. Immunol. 2016; 7:684. Available from: URL: https://www.frontiersin.org/journals/immunology/articles/10.3389/fimmu.2016.00684/full.
90. Brown FD, Turley SJ. Fibroblastic reticular cells: organization and regulation of the T lymphocyte life cycle. J Immunol 2015; 194:1389–94.
91. Baptista AP, Roozendaal R, Reijmers RM, Koning JJ, Unger WW, Greuter M et al. Lymph node stromal cells constrain immunity via MHC class II self-antigen presentation. Elife 2014; 3.

Figures

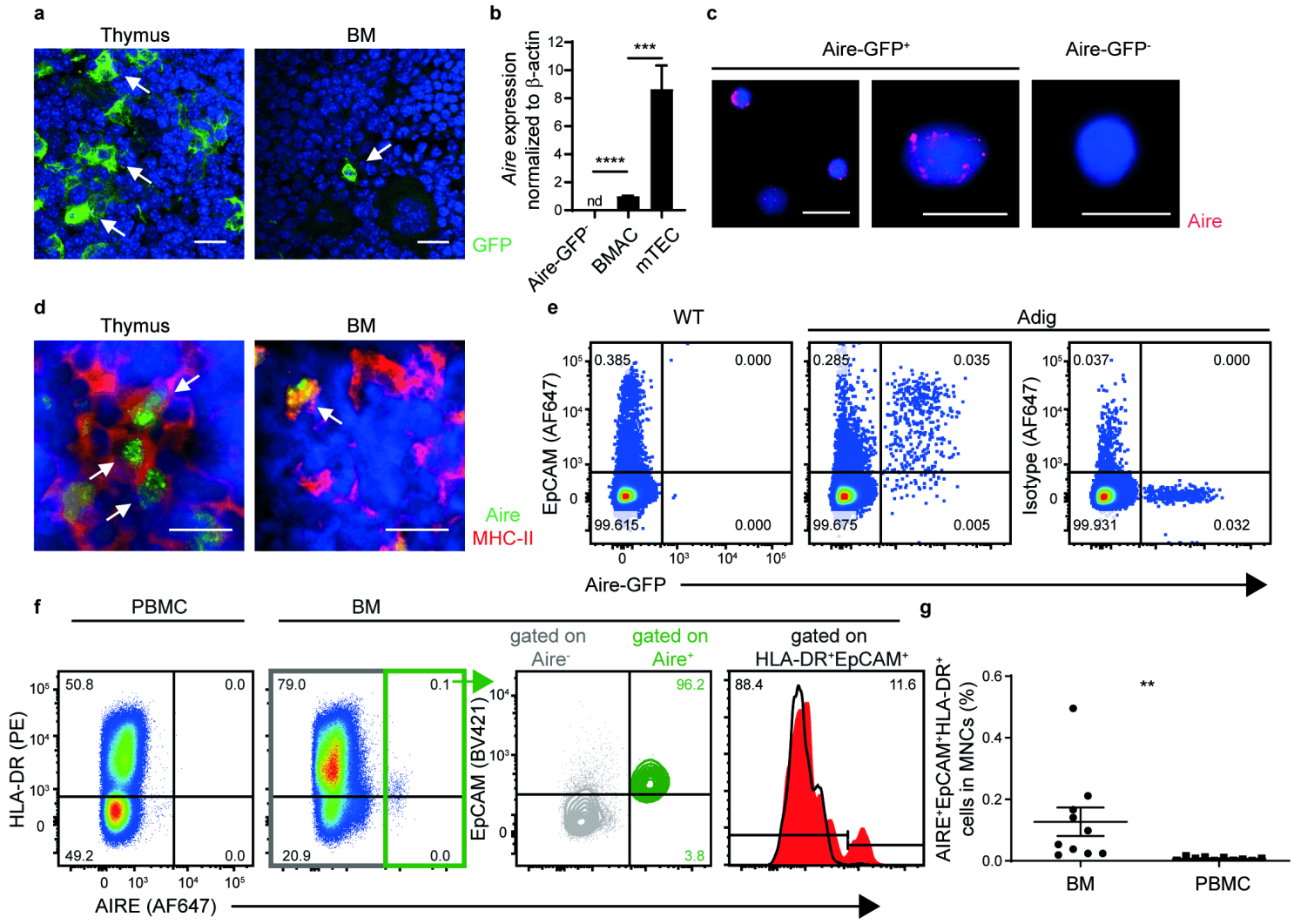


Figure 1

Aire expression in murine and human MHC-II^{+}EpCAM^{+} BM cells.

(A) Immunofluorescence of GFP on thymus and BM tissue of Adig mice. Arrows indicate Aire-GFP expressing cells. **(B)** Real-Time PCR analysis of *Aire* transcript expression in sorted Aire-GFP^{+} BMACs, Aire-GFP^{-} BM cells and mTECs from Adig mice. Data were normalized to b-actin. ***, $P < 0.001$; ****, $P < 0.0001$ (Student's *t*-test). **(C)** Immunocytochemistry of Aire on Adig BM cells sorted by GFP expression. **(D)** Immunofluorescence of Aire and MHC-II on thymus and BM tissue of WT Balb/c mice. Arrows indicate Aire-expressing cells. **(E)** Flow cytometric analysis of EpCAM expression on total BM cells of Adig mice (n = 5). Frequencies of cells in each quadrant are shown in percentage. **(F)** Gating strategies for AIRE-expressing cells in human BM cells and PBMCs. Gray population represents Aire^{-} cells; green population represents Aire^{+}HLA-DR^{+} cells. Histogram shows Aire expression in HLA-DR^{+}EpCAM^{+}_ cells; unshaded curve in histogram indicates isotype control. Frequencies of gated cells are shown in percentage. **(G)** Frequencies of AIRE^{+}EpCAM^{+}HLA-DR^{+} cells in mononuclear cells (MNCs) in BM and blood (mean ± SEM), evaluated according to the gating strategy shown in (F). Scale bars indicate 15 μm

(A,C,D). **, $P < 0.01$ (paired Student's *t*-test). Data are representative of two (A,C,D) or three (E) independent experiments, or accumulated from five experiments (B) or ten donors (G).

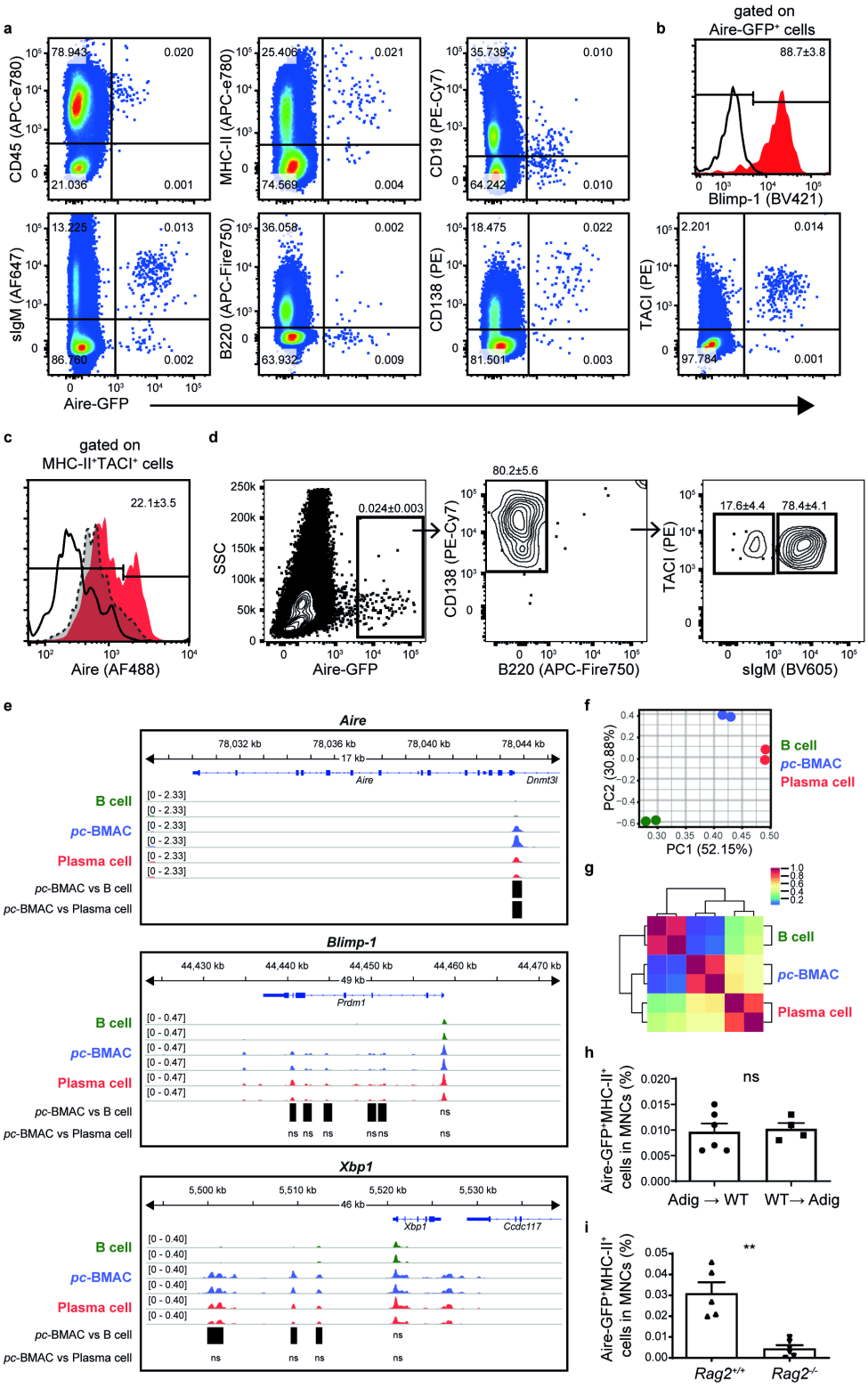


Figure 2

BMACs show plasma cell features.

(A) Flow cytometric analysis of surface marker expression on total BM cells of Adig mice (n = 4). Frequencies of cells in each quadrant are shown in percentage. sIgM, surface IgM. **(B)** Intracellular Blimp-1 staining on Aire-GFP^{+} BM cells. Unshaded curve indicates isotype control (n = 3). **(C)** Intracellular Aire staining on MHC-II^{+}TACI^{+} BM cells from *Aire*$^{+/+}$ (solid red curve) or *Aire*$^{-/-}$ (dotted gray curve) mice. Unshaded curves indicate isotype control of *Aire*$^{+/+}$ mice (n = 3). **(D)** Gating strategy for *pc*-BMACs in Adig mice. **(E)** Chromatin accessibility of *Aire*, *Prdm1*, and *Xbp1* loci in *pc*-BMACs, B cells (CD138^{-}B220^{hi}) and plasma cells (CD138^{+}TACI^{+}B220^{-}) in the BM. Gene information and genomic location is shown on top. All samples are group-normalized to allow peak height comparison (scale of ATAC-seq signal shown in brackets). Bars below represent significant peaks between the compared groups. **(F,G)** PCA (F) and unsupervised clustering (G) of accessible chromatin regions of cell subsets as in (E). **(H)** Frequencies of Aire-GFP^{+}MHC-II^{+} cells among BM mononuclear cells (MNCs) of reciprocal BM chimeras: Adig→WT (n = 6) and WT→Adig (n = 4) (mean ± SEM). **(I)** Frequencies of Aire-GFP^{+}MHC-II^{+} cells among BM MNCs of RAG2$^{+/+}$ (n = 5) and RAG2$^{-/-}$ (n = 6) Adig mice (mean ± SEM). In (B-D), frequencies of gated populations are shown in percentage (mean ± SEM). **, $P < 0.01$; ns, $P > 0.05$ (Student's t-test). Data are representative of three (A,B,D) or two independent experiments (C,E-I).

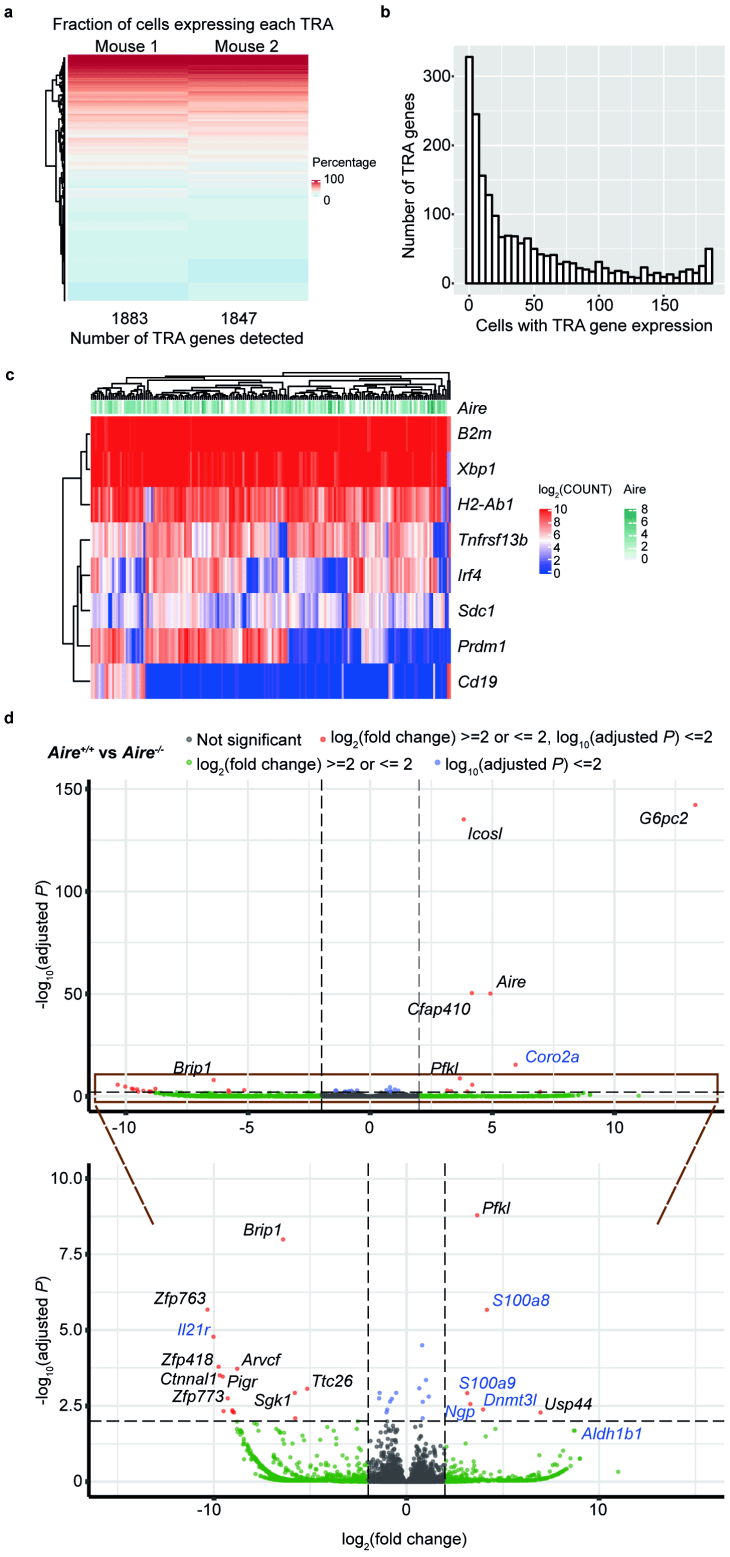


Figure 3

pc-BMACs express TRA genes and genes related to immune regulation.

(A) TRA genes color-coded for the fraction of single *pc*-BMACs expressing each TRA gene. Numbers of TRA genes detected in each *Aire*$^{+/+}$ mouse are indicated. **(B)** Amount of TRA genes as a function of the number of single *pc*-BMACs (n = 186) for which the expression of the TRA genes was detected. **(C)**

Heatmap of expression levels of plasma cell-related genes in individual *pc*-BMACs. Expression levels of *Aire* for individual cells are annotated. **(D)** Volcano plots of genes differentially expressed in bulk *pc*-BMACs in *Aire*$^{+/+}$ mice compared to bulk *pc*-BMACs in *Aire*$^{-/-}$ mice. Lower plot shows the designated region (brown rectangle) of the upper plot. TRA genes are labeled in blue.

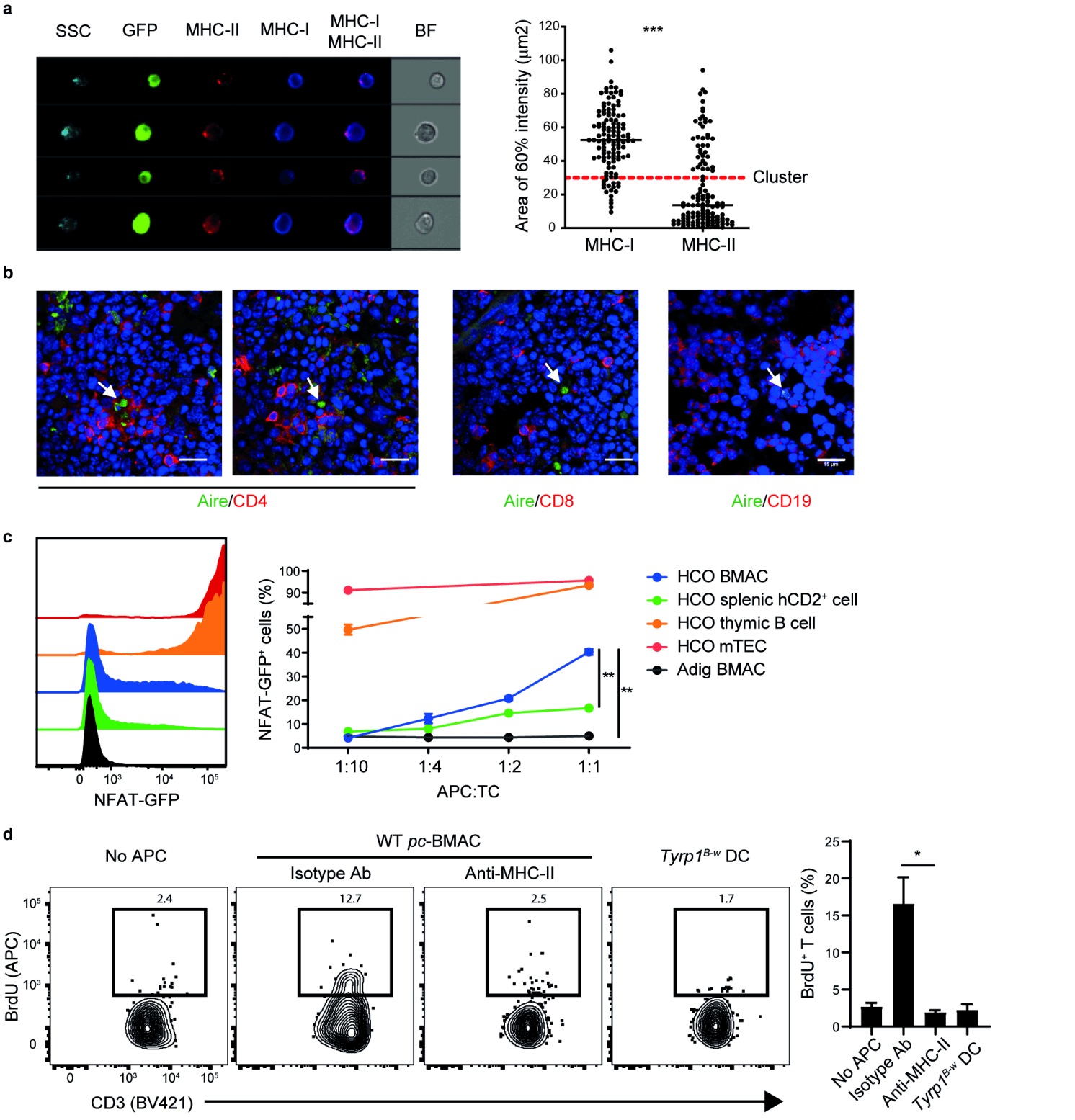


Figure 4

BMACs present Aire-driven transgenic antigen and endogenous TRA to CD4$^+$ T cells.

(A) Multispectral imaging flow cytometric analysis of MHC-I and MHC-II expression on Aire-GFP$^+$ BMACs of Adig mice. The areas containing 60% of the respective MHC intensity are depicted, and the expression of MHC molecules with an area below 30 μm^2 is defined as clustered. Black bars represent the median. SSC, side scatters. BF, bright field. **(B)** Immunofluorescence of Aire and CD4, CD8 or CD19 on BM tissue of WT Balb/c mice. Arrows indicate BMACs. Scale bar indicates 15 μm. **(C)** Presentation of HA antigen to A5 T-hybridoma cells by designated subsets of APCs from Aire-HCO or Adig mice at different APC:TC ratios. Representative histogram of NFAT-GFP expression at 1:1 APC:TC ratio is shown. Data are pooled from two independent experiments (n ≥ 3, mean ± SEM). **(D)** BrdU incorporation of Tyrp1 specific CD4$^+$ T cells after co-culture with *pc*-BMACs sorted from WT B6 or CD11c$^+$ dendritic cells from Tyrp1-deficient (*Tyrp1*$^{B\text{-}w}$) mice in the presence of anti-MHC-II antibody (clone Y-3P) or isotype control antibody. Numbers indicate percentages of gated cells among CD3$^+$ T cells. ***, $P < 0.001$; *, $P < 0.05$ (Student's *t*-test). Data are representative of two independent experiments (n = 3, mean ± SEM).

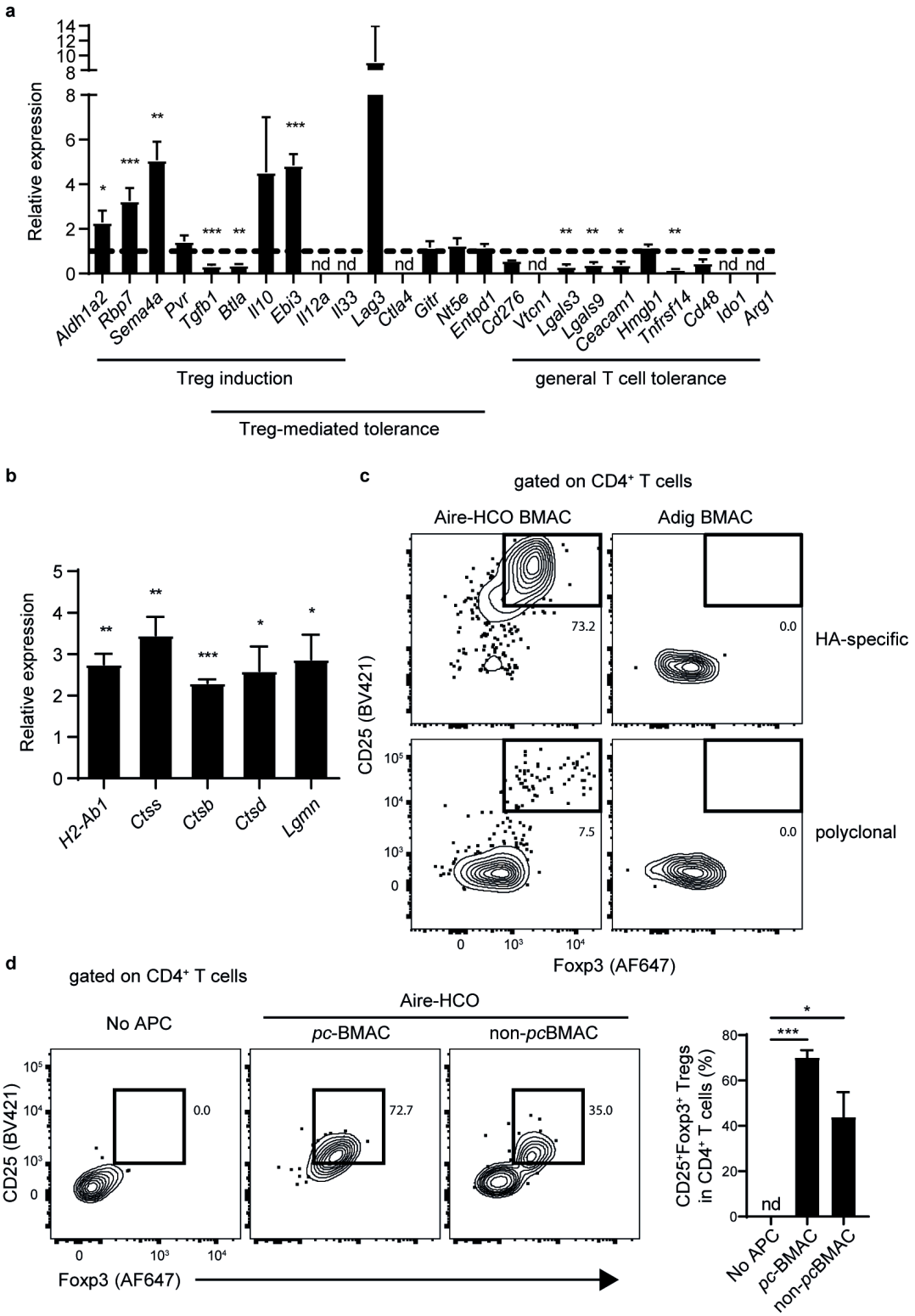


Figure 5

BMACs selectively express Treg induction-associated genes and induce conversion of Treg cells *in vitro*.

(A,B) Relative mRNA expression of genes associated with immune tolerance (A) or with MHC-II antigen presentation (B) in *pc*-BMACs compared to BM plasma cells of Adig mice by gene expression array

analysis (mean ± SEM). **(C)** Frequencies of CD25$^+$Foxp3$^+$ cells among CD4$^+$ cells after co-culture with BMACs from Aire-HCO or Adig mice (n = 3). **(D)** Frequencies of CD25$^+$Foxp3$^+$ cells among HA-specific CD4$^+$ cells after co-culture with *pc*-BMACs or non-*pc*BMACs from Aire-HCO mice (n = 3, mean ± SEM). *, $P < 0.05$; **, $P < 0.01$; ***, $P < 0.001$; nd, not detected. Data are representative of two independent experiments (C,D).

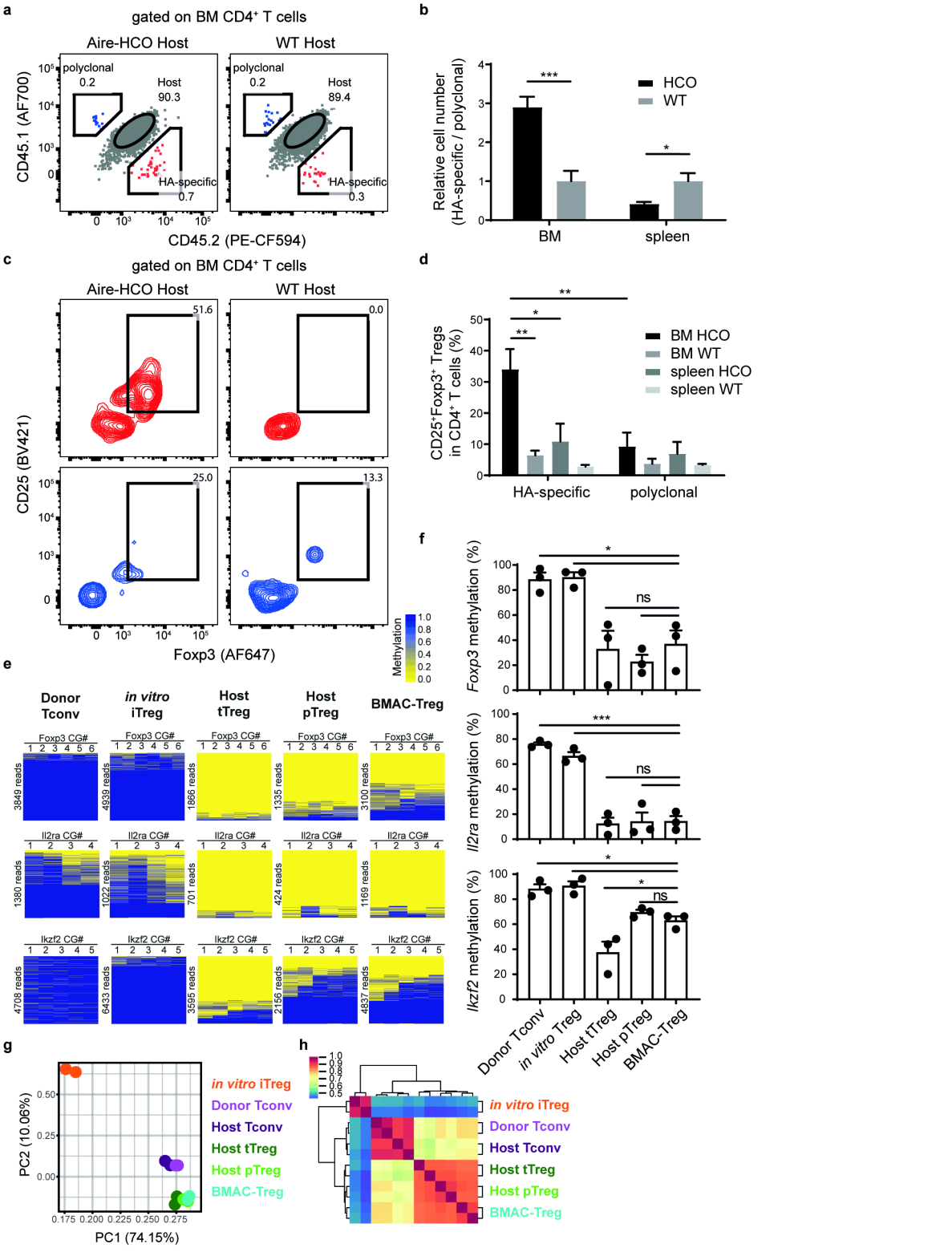


Figure 6

BMACs induce conversion of naïve CD4 T cells to *bona fide* Treg cells *in vivo*.

(A,B) Representative frequencies (A) of CD45.2$^+$ HA-specific (red) and CD45.1$^+$ polyclonal CD4$^+$ T cells (blue) and ratio of HA-specific/polyclonal T cells (B) on day 14 post-transfer (n = 4, mean ± SEM). **(C,D)** Representative (C) and summary (D) of frequencies of CD25$^+$Foxp3$^+$ Treg cells in CD45.2$^+$ HA-specific (red) and CD45.1$^+$ polyclonal CD4$^+$ T cells (blue) on day 14 post-transfer (n = 4, mean ± SEM). Numbers indicate percentages among HA-specific or polyclonal CD4$^+$ T cells as in (A). **(E,F)** Representative (E) and summary (F) of CG methylation status of *Foxp3* TSDR, *Il2ra*, and *Ikzf2* loci in BMAC-Tregs (CD45.2$^+$CD25$^+$Foxp3$^+$), Donor Tconvs (CD45.2$^+$CD25$^-$Foxp3$^-$), Host tTregs (CD25$^+$Foxp3$^+$Helios$^+$) and Host pTregs (CD25$^+$Foxp3$^+$Helios$^-$) from BM CD4$^+$ T cells, as well as *in vitro* iTregs. Total numbers of reads are annotated for each plot. Columns indicate CG sites (see *Materials and Methods* for precise genomic location), and rows indicate individual reads (n = 3, mean ± SEM). **(G,H)** PCA (G) and unsupervised clustering (H) of accessible chromatin regions by ATAC-seq from BMAC-Tregs (CD45.2$^+$CD25$^+$LAP$^+$), Donor Tconvs (CD45.2$^+$CD25$^-$), Host tTregs (CD25$^+$CTLA-4$^+$Nrp1$^+$), and Host pTregs (CD25$^+$CTLA-4$^+$Nrp1$^-$) from BM CD4$^+$ T cells, as well as *in vitro* iTregs. ns, $P > 0.05$; *, $P < 0.05$; **, $P < 0.01$; ***, $P < 0.001$ (Student's *t*-test in (B,D) and one-way-ANOVA with Tukey's multiple comparisons test in (F). Data are representative of three (A-D) or two independent experiments (E-H).

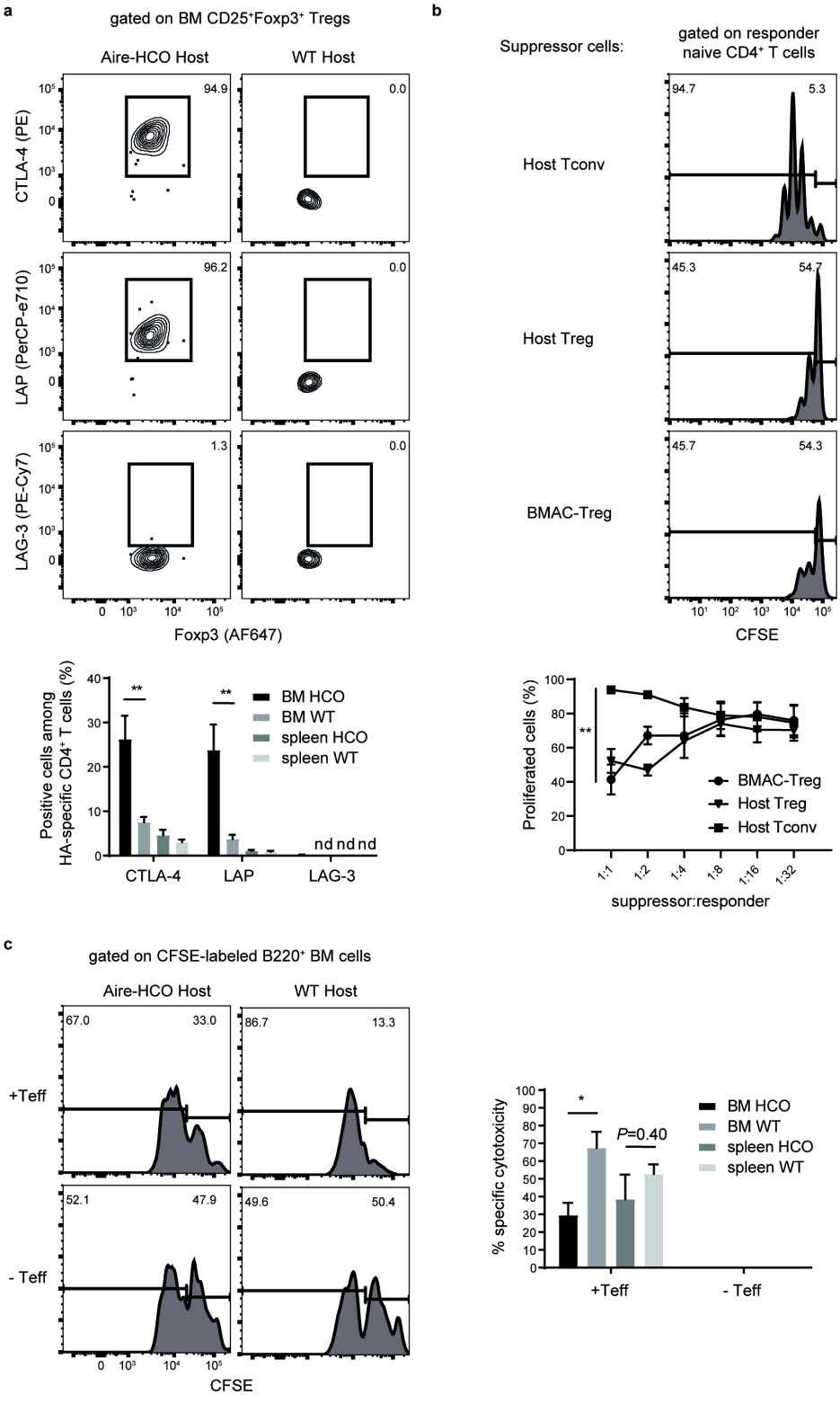


Figure 7

BMAC-induced Treg show activated phenotype and suppressive function.

(A) Representative and summary the frequencies of CTLA-4$^+$, LAP$^+$ and LAG-3$^+$ HA-specific Tregs in the BM or spleen of Aire-HCO or WT hosts on day 14 post-transfer (n = 4, mean ± SEM). Numbers in contour plots indicate percentages among CD25$^+$Foxp3$^+$ Tregs. **(B)** Suppression of naïve responder T cell

proliferation co-cultured with BMAC-Tregs, Host Tregs and Host Tconvs (sorted as in **Figure 6G, H**) at different ratios of suppressor:responder cells (n = 3, mean ± SEM). Representative histograms show reduced CFSE fluorescence intensity as indication of proliferation of responder T cells at the suppressor:responder ratio of 1:1. **(C)** Frequencies of $B220^{+}CFSE^{high}$ and $B220^{+}CFSE^{low}$ target cells and specific cytotoxicity (18 hours after target cell transfer) in the BM or spleen of Aire-HCO or WT hosts with or without co-transfer of HA-specific effector T cells. Numbers in histograms indicate percentages of gated $B220^{+}$ cells (n = 3, mean ± SEM). nd, not detected. *, $P < 0.05$; **, $P < 0.01$ (Student's *t*-test). Data are representative of three (A) or two (B,C) independent experiments.

Supplementary Files

This is a list of supplementary files associated with this preprint. Click to download.

- supplementaryTableS2.xlsx
- supplementaryTableS1.xlsx
- Unprocessedoriginalimages.pdf
- Supplement.pdf